catalysts

MDPI

Review

Proton-Exchange Membrane Electrolysis for Green Hydrogen Production: Fundamentals, Cost Breakdown, and Strategies to Minimize Platinum-Group Metal Content in Hydrogen Evolution Reaction Electrocatalysts

Henrique F. Araújo, Julián A. Gómez and Diogo M. F. Santos *

Center of Physics and Engineering of Advanced Materials, Laboratory for Physics of Materials and Emerging Technologies, Chemical Engineering Department, Instituto Superior Técnico, Universidade de Lisboa, 1049-001 Lisbon, Portugal; henrique.f.araujo@tecnico.ulisboa.pt (H.F.A.); julian.gomez.mayorga@tecnico.ulisboa.pt (J.A.G.)
* Correspondence: diogosantos@tecnico.ulisboa.pt

Abstract: Green hydrogen (H_2) has emerged as a promising energy carrier for decarbonizing the industrial, building, and transportation sectors. However, current green H_2 production technologies face challenges that limit cost reduction and scaling up. Platinum-group metals (PGMs), including platinum and iridium, present exceptional electrocatalytic properties for water splitting, but their high cost is a significant barrier. This directly impacts the overall cost of electrolyzers, thus increasing green H_2 production costs. The present work covers the fundamentals of water electrolysis, the currently available technologies, focusing on proton-exchange membrane electrolyzers, and the critical role of electrocatalysts, discussing potential strategies for reducing the PGM content and, consequently, decreasing green H_2 cost.

Keywords: green hydrogen; hydrogen evolution reaction; PEM electrolyzer; water electrolysis; platinum-group metals; electrocatalysts

Citation: Araújo, H.F.; Gómez, J.A.; Santos, D.M.F. Proton-Exchange Membrane Electrolysis for Green Hydrogen Production: Fundamentals, Cost Breakdown, and Strategies to Minimize Platinum-Group Metal Content in Hydrogen Evolution Reaction Electrocatalysts. *Catalysts* **2024**, *14*, 845. https://doi.org/10.3390/catal14120845

Academic Editor: Annalisa Vacca

Received: 6 November 2024
Revised: 19 November 2024
Accepted: 20 November 2024
Published: 22 November 2024

1. Introduction

The global energy demand is projected to increase dramatically over the next few decades. The expected increase in the world's population, as well as the relentless pace of economic and industrial progress of non-developed and developed countries, are the main causes of this problem. Currently, 76% of the energy demand is met by fossil fuels [1]. Fossil fuels also account for over 75% of global greenhouse gas emissions and nearly 90% of the total CO_2 emissions [2]. Renewable energy sources (RES) have emerged as promising and sustainable solutions to mitigate the climate crisis due to their low environmental impact. Hydro, wind, solar, and traditional biomass technologies stand out as leading contributors to global renewable energy production [1]. However, there are obstacles to overcome to maximize renewables' share in the global energy mix.

One of the most important challenges is the inherent fluctuation of RES output. Predicting renewable energy generation is subject to errors due to the inherent uncertainty in weather forecasting. It can be difficult to accurately estimate and balance the supply and demand of energy since variables like precipitation, wind speed, fluctuations in temperature, and sunlight availability can affect how much energy is produced. To address this challenge, hydrogen (H_2) stands out as a versatile solution capable of managing this variability. By harnessing surplus electricity generated from RES to drive water electrolyzers and produce H_2 as an energy carrier, renewables can significantly improve their contribution to the energy landscape.

H_2 has the potential to revolutionize the way we produce, store, and transport energy from RES. According to the International Renewable Energy Agency (IRENA), the current

global H_2 production is approximately 120 Mt, with two-thirds being pure H_2 and the remaining one-third being mixed with other gases [3,4]. H_2 production currently relies heavily on fossil fuels, with natural gas and coal serving as the primary energy sources. As of the end of 2021, it was estimated that approximately 47% of global H_2 production came from natural gas, 27% from coal, 22% from oil as a by-product, around 3% was produced through electrolysis using the electrical grid, and less than 1% was produced using renewable energy [4,5]. Splitting water into H_2 and oxygen (O_2) using renewable electricity is the core process for green H_2 production.

Traditionally, the major cost of green H_2 production is related to the price of renewable electricity. As solar photovoltaic and wind electricity costs have consistently decreased over the years, renewable energy has become more accessible and affordable [6]. This shift has transformed the landscape, with the cost associated with electrolyzers now taking center stage as the primary cost contributor in the renewable H_2 production system. One of the most important challenges is the need for further technological advancements to enhance the overall performance of electrolyzers. This enhancement should improve efficiency and lifetime, ensuring these systems operate optimally over extended periods [7]. The efficiency of electrolyzers is crucial in maximizing the H_2 yield per unit of input energy, thereby reducing costs and environmental impact.

In addition to technological advancements, implementing H_2 policies is crucial to achieving economies of scale, enabling a cost reduction in green H_2 production. These regulations are key in developing favorable conditions for green H_2 projects, encouraging investment, and promoting market expansion [8]. In 2023, the Hydrogen Council has estimated that a cumulative electrolysis capacity exceeding 230 GW is set to become operational by 2030 (Figure 1). To achieve this ambitious goal, a remarkable 300-fold increase in deployment would be required over the next 7 years [9].

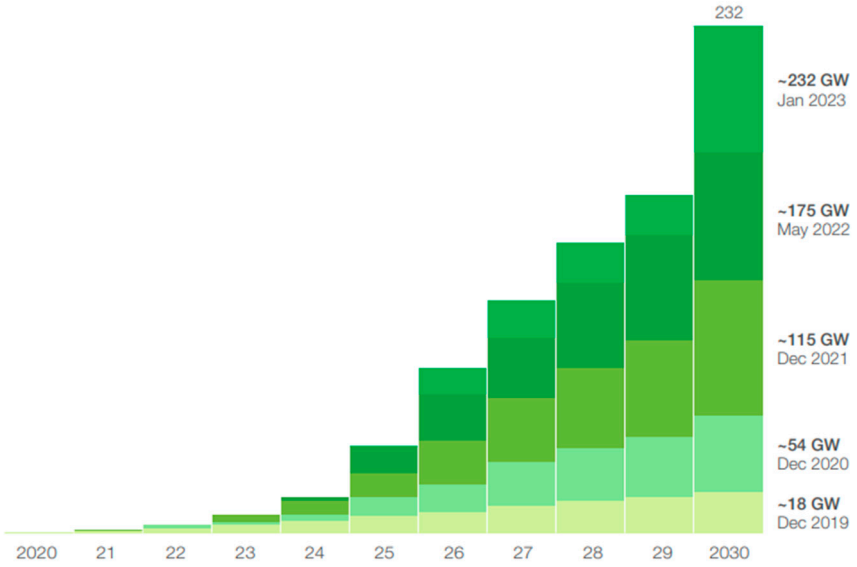

Figure 1. Estimated global electrolysis capacity (GW), including all project maturity stages [9].

Furthermore, the cost of electrocatalysts, particularly those based on platinum-group metals (PGMs), poses a significant challenge. PGMs, such as platinum (Pt), palladium (Pd), rhodium (Rh), iridium (Ir), and ruthenium (Ru), are essential materials due to their exceptional electrocatalytic properties for the water-splitting process. However, their high cost directly impacts the overall cost of electrolyzers and, consequently, the cost of green H_2 production [7]. The water electrolysis process can be divided into two half-cell reactions: hydrogen evolution reaction (HER) and oxygen evolution reaction (OER). These reactions are inherently constrained by kinetic and thermodynamic limitations, resulting in sluggish charge transfer and relatively low reaction rates [10]. The water-splitting process occurs at considerably high cell potentials, typically in the 1.8–2.0 V range for commercial

electrolyzers. Notably, this voltage range is about 0.55 to 0.77 V higher than the theoretical thermodynamic value (E°_{cell} = 1.229 V) required for water splitting. This excess potential, referred to as overpotential (η), is essential to overcome the energy barrier of the reaction system and drive the electrochemical process [11]. In this context, electrocatalysts alter the reaction kinetics by providing alternative reaction pathways with lower activation energy. These pathways enhance the charge transfer during HER and OER, thus improving reaction kinetics. Consequently, these processes can occur at lower overpotentials, thus reducing the overall energy consumption of the process [10].

This review aims to comprehensively analyze the electrochemistry fundamentals of water splitting in acidic conditions. It also thoroughly reviews proton-exchange membrane electrolyzers (PEMEL), their primary components, and operating principles. Furthermore, it explores the role of electrocatalysts and recent advances to enhance the HER performance. The work is structured as follows. Section 1 discussed the importance of green H_2 in the energy transition, along with the scope and motivation of this review. Section 2 presents the fundamentals of the water electrolysis process, covering aspects such as the relevant half-reactions and the performance evaluation indexes for electrochemical systems. Section 3 comprehensively reviews PEMEL technology, including its working principles, main components, costs, and market considerations. Section 4 provides a review of electrocatalysts for HER, as well as current strategies to minimize precious metal content. Finally, the last section comprises a discussion and the main conclusions drawn from the study.

2. Fundamentals of Water Electrolysis

Water electrolysis is a chemical process that involves splitting water molecules (H_2O) into their constituent elements, H_2 and O_2, using an electrical current. Equations (1) and (2) give the two half-cell reactions involved in the electrical-driven water-splitting process for acidic media, with Equation (3) being the global reaction.

$$\text{Cathode}: \ 2H^+ + 2e^- \ \rightarrow \ H_{2(g)} \qquad E^{\circ}_{c} \ = \ 0.000 \text{ V vs. SHE} \tag{1}$$

$$\text{Anode}: \ 2H_2O_{(l)} \ \rightarrow \ O_{2(g)} + 4H^+ + 4e^- \qquad E^{\circ}_{a} \ = \ 1.229 \text{ V vs. SHE} \tag{2}$$

$$\text{Overall}: \ 2H_2O_{(l)} \ \rightarrow \ 2H_{2(g)} + O_{2(g)} \qquad E^{\circ}_{cell} = -1.229 \text{ V vs. SHE} \tag{3}$$

Equation (1) corresponds to the HER, in which the available free H^+ protons are reduced at the cathode to produce H_2, while Equation (2) represents the OER, where water is oxidized at the anode to produce O_2 [12]. The standard equilibrium voltage of the overall reaction, E°_{cell}, is given by the difference between the standard electrode potentials at the cathode, E°_{c}, and the anode, E°_{a}, and is equal to −1.229 V under standard temperature and pressure conditions (T = 298 K, P = 1 atm) and pH = 0 [13]. The negative equilibrium potential indicates a nonspontaneous cell reaction that must be driven by imposing an external cell voltage greater than 1.229 V.

The Nernst equation can estimate the equilibrium voltage for conditions different from STP. It states that the equilibrium voltage is determined by standard equilibrium voltage and a term that depends on the temperature and the concentration, activities, or partial pressures of reactants and products. For a reaction given by aA + bB → cC + dD, the Nernst equation can be expressed as Equation (4),

$$E = E^{\circ} - 2.303 \, \frac{RT}{nF} \log \frac{[A]^a \, [B]^b}{[C]^c \, [D]^d} \tag{4}$$

where R = 8.314 J mol^{-1} K^{-1} is the ideal gas constant, T is the temperature at which the reaction is taking place, n is the number of transferred electrons (for water electrolysis, n = 2 for HER and n = 4 for OER), F = 96,485 C mol^{-1} is the Faraday constant, and [A], [B], [C] and [D] represent the concentration, activity or partial pressure of the involved species.

When applying the Nernst equation to the half reactions of the water electrolysis in acidic media, it results in Equations (5) and (6),

$$E_c = E_c^{\circ} - 2.303 \frac{RT}{2F} \log \frac{P_{H_2}}{[H^+]^2} \quad (5)$$

$$E_a = E_a^{\circ} + 2.303 \frac{RT}{4F} \log P_{O_2} [H^+]^4 \quad (6)$$

where $[H^+]$ is the concentration of hydrogen ions, and PH_2 and PO_2 are the partial pressures of H_2 and O_2, respectively. As shown in Equations (5) and (6), the pH value of the electrolyte solution plays a critical role in determining the electrode potential values necessary to achieve a certain current density. Variations in pH can substantially impact the reaction kinetics. Figure 2 presents the Pourbaix diagram of water, showing the stability regions of water in terms of pH and electrode potential [14].

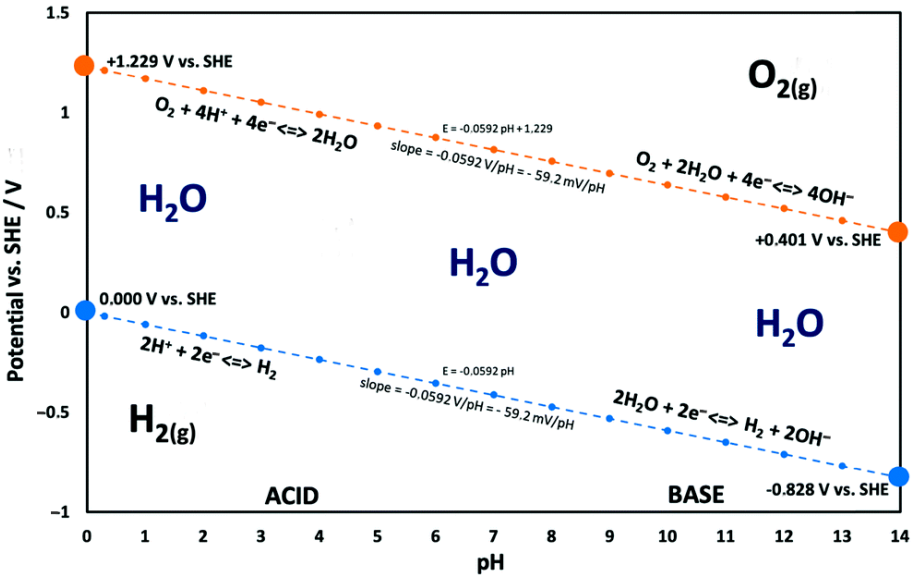

Figure 2. Pourbaix diagram of water (adapted from [14]).

Pourbaix diagrams can be thought of as electrochemical phase diagrams, mapping out zones of thermodynamic stability for substances involved in redox reactions. Just like traditional phase diagrams, these diagrams use lines to delineate the conditions at which two phases coexist in equilibrium. In the case of the water Pourbaix diagram, the region between the dotted lines illustrates the potential and pH conditions where liquid water remains stable. Beyond the area delimited by the two lines, water becomes thermodynamically unstable and either gets reduced to form $H_{2(g)}$ (below the blue line) or oxidized to produce $O_{2(g)}$ (above the orange line) [15].

A fundamental parameter that characterizes the performance of both HER and OER is the overpotential (η). It is defined as the difference between the actual electrode potential ($E_{HER|OER}$) and the thermodynamic equilibrium potential ($E^{\circ}_{HER|OER}$) [14]. Oxygen-evolving electrodes, in particular, incur a significantly higher overpotential ($\eta_{OER} = E_{OER} - E^{\circ}_{OER}$) under neutral or acidic conditions than under alkaline conditions. Contrary to this, the overpotential in hydrogen-evolving electrodes ($\eta_{HER} = E_{HER} - E^{\circ}_{HER}$) is higher in neutral and alkaline conditions. It is clear then that depending on the value of the electrode potential relative to the equilibrium electrode potential, either the forward reaction or the reverse reaction of each electrode reaction is slowed down or accelerated. In this way, at the anode, the oxidation half-reaction will be accelerated by an electrode potential that exceeds the equilibrium potential of the OER ($\eta_{OER} > 0$), and at the cathode, the reduction

half-reaction will be accelerated by an electrode potential that is more negative than the equilibrium electrode potential of the HER, ($\eta_{HER} < 0$) [14].

Another important parameter is the energy efficiency, ε, of the water-splitting reaction (Equation (7)). It can be quantified by dividing the thermodynamic equilibrium cell voltage (E°_{cell} = 1.229 V, STP) by the actual cell voltage, E_{cell}. This real cell voltage is measured while the system operates at specific T, P, and current density, j. This parameter evaluates how efficiently the reaction converts energy under realistic working conditions.

$$\varepsilon = \frac{E^{\circ}_{cell}}{E_{cell}} \quad (7)$$

Furthermore, from a thermodynamic point of view, the water-splitting reaction is an endothermic reaction ($\Delta H > 0$), suggesting that splitting 1 mol of liquid H_2O to produce 1 mol of H_2 under STP requires a certain amount of energy. This can be explained by the relation expressed in Equation (8),

$$\Delta H^{\circ} = \Delta G^{\circ} + T\ \Delta S^{\circ} \quad (8)$$

where the change in the Gibbs free energy (ΔG°) is 237.1 kJ/mol and the thermal energy ($T\ \Delta S^{\circ}$) is 48.7 kJ/mol under STP [13]. The theoretical total amount of energy (ΔH°) required to drive the electrolysis process is 285.8 kJ/mol. Both thermal and electrical energy contribute to the total energy requirement. Equation (9) shows an alternative expression of the water-splitting reaction under STP derived from the previously mentioned thermodynamic principle.

$$H_2O_{(liq)} + 237.1\ kJ/mol(electricity) + 48.8\ kJ/mol(heat) \rightarrow H_{2(g)} + ½O_{2(g)} \quad (9)$$

Based on the reaction stoichiometry, producing 1 kg of H_2 via electrolysis requires 9 L of H_2O and results in the creation of 8 kg of O_2 as a by-product [16]. The following sections delve deeper into the HER and OER mechanisms for heterogeneous electrocatalysis in acidic media. Understanding the mechanism behind these reactions permits the identification of the key steps that need to be enhanced to improve the efficiency of the water-splitting process.

2.1. Hydrogen Evolution Reaction (HER)

The HER is a multi-step electrochemical process that takes place at the electrode surface. The first step involves the discharged protons' adsorption on an active electrode site. The so-called "Volmer step" is characterized by the simultaneous adsorption of a proton on an unoccupied electrode active site and an electron transfer from the electrode to the proton, resulting in the adsorption of a hydrogen atom (Equation (10)). For acidic conditions, the proton source is the hydrogen ion (H^+) [11,17],

$$H^+ + e^- \rightarrow H^* \quad (\text{Volmer step}) \quad (10)$$

where H* stands for a H atom adsorbed on the electrocatalyst active site. The second step involves the desorption of H_2 from the cathode through one of two different possible pathways: electrochemical (Heyrovský step, Equation (11)) or chemical (Tafel step, Equation (12)). In the Heyrovský step, the transfer of a second electron to the adsorbed hydrogen atom comes together with the transfer of another proton from the solution to produce H_2. On the other hand, the Tafel step involves the combination of two already adsorbed hydrogen atoms on the electrode surface to produce H_2 [11,14,17].

$$H^+ + e^- + H^* \rightarrow H_2 \quad (\text{Heyrovský step}) \quad (11)$$

$$H^* + H^* \rightarrow H_2 \quad (\text{Tafel step}) \quad (12)$$

Figure 3 schematically represents the HER through the two different pathways. In this case, the blue arrows represent the Volmer step on the active site of the electrode, the purple arrows represent the Heyrovský step, where a second electron interacts with the adsorbed hydrogen, and the red arrows represent the Tafel step, where two adsorbed hydrogen atoms are combined on the surface electrode.

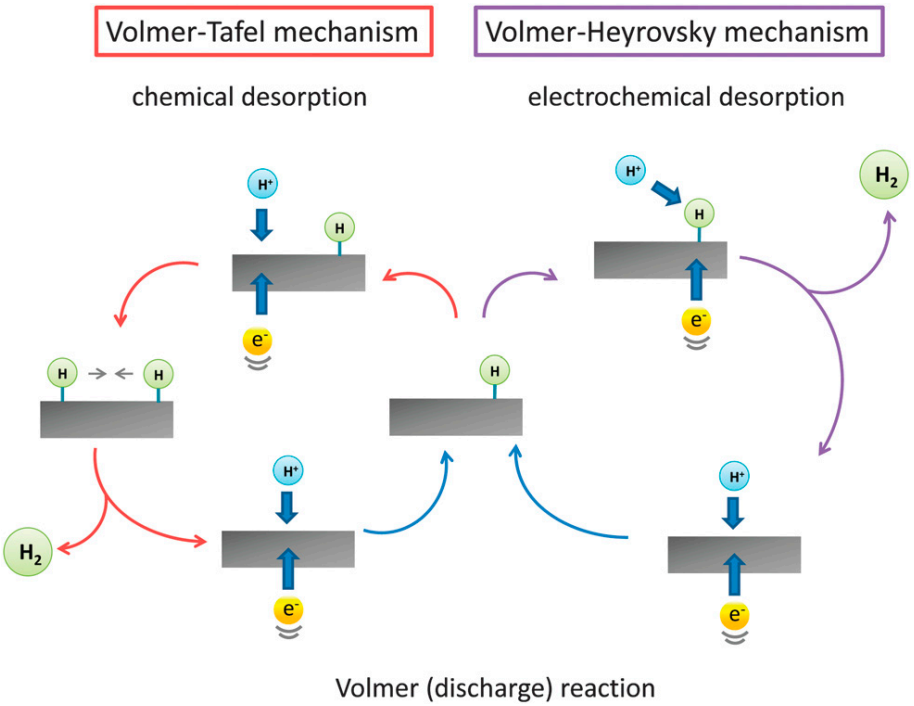

Figure 3. HER mechanisms on the electrode surface for acidic conditions [17]. Reprinted with permission from the Royal Society of Chemistry.

Determining the rate-controlling step, and thus the predominant mechanism, in the HER process can be simplified by evaluating the Tafel slope value from the HER polarization curve. Tafel slope values for the Volmer, Heyrovský, and Tafel steps can be expressed by Equations (13)–(15), respectively [11],

$$b_V = \frac{2.303\ R\ T}{\alpha\ F} \quad (13)$$

$$b_H = \frac{2.303\ R\ T}{(1+\alpha)F} \quad (14)$$

$$b_T = \frac{2.303\ R\ T}{2\ F} \quad (15)$$

where b represents the Tafel slope value (b_V for the Volmer step, b_H for the Heyrovský step, and b_T for the Tafel step), R is the ideal gas constant, T denotes the temperature, F is the Faraday constant, and α is the symmetry coefficient (set to 0.5). The reference values for each step are 120 mV/dec, 40 mV/dec, and 30 mV/dec for the Volmer, Heyrovský, and Tafel steps, respectively. Notably, the lower the Tafel slope value, the faster the reaction kinetics [11].

Experimentally obtained Tafel slopes are frequently compared to the theoretical values obtained via microkinetic models to identify the rate-determining step (RDS) of HER catalyzed by a given electrocatalyst material. However, the Tafel slopes estimated by those models frequently use extreme assumptions, such as complete active site coverage or almost zero site coverage of intermediates, when, in fact, site occupation is potential-dependent, which also alludes to the potential-dependent nature of reaction rates. As such,

these assumptions lead to inaccuracies in the description of the surface kinetics, and the supposed identification of the RDS may not be significant.

Simulated theoretical data with microkinetic models that consider complete surface coverage phenomena have shown that the Tafel slope values frequently attributed to the Volmer step when it acts as the RDS could also be attributed to the Heyrovský step with a high surface coverage acting as the RDS. This also applies to other relevant electrochemical reactions, such as the OER, oxygen reduction reaction, and hydrogen oxidation reaction. Nevertheless, using Tafel slopes to determine the RDS should be performed with caution [18].

Finally, by using the Gibbs free energy concept for H* adsorption (ΔGH*) on an electrocatalyst surface, the assessment of both H* adsorption and H desorption can be performed. The efficiency and performance of electrocatalysts in the HER are intricately related to the ΔGH*. This parameter is calculated from density functional theory and experimentally plotted against the logarithm of exchange current densities (log j_0) for a diverse number of electrocatalysts, providing valuable insights into their electrocatalytic activity [11,17]. As shown in Figure 4, the relationship between exchange current densities, j_0, and ΔGH* exhibits a volcano shape where PGMs, positioned at the peak, possess the highest activity and the ideal (i.e., intermediate) hydrogen adsorption energy.

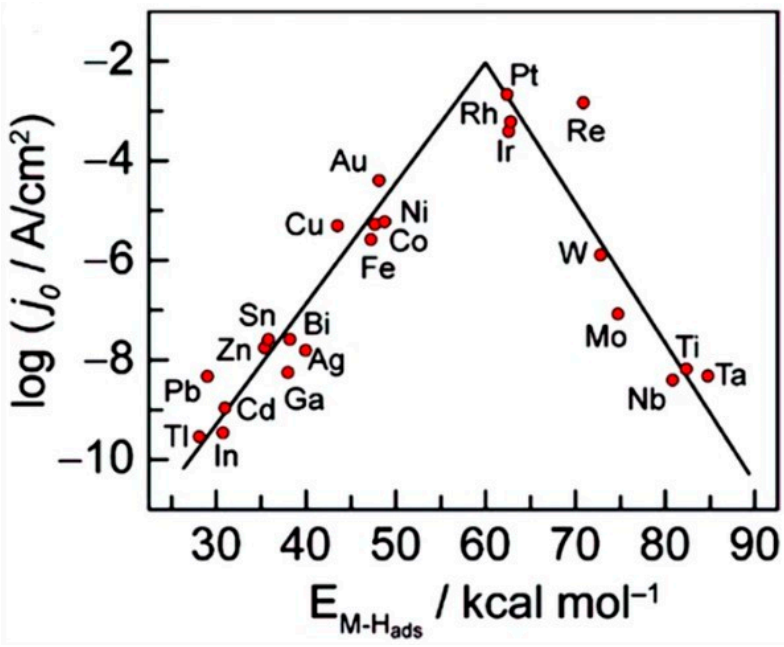

Figure 4. HER volcano plot for metal electrodes under acidic conditions. For each metal, the logarithm of j_0 is plotted against the metal-hydrogen bond energy $E_{M\text{-}H_{ads}}$ [11].

This information, rooted in the Sabatier principle, which states that the binding energy between the electrocatalyst and the reactant should be neither too strong nor too weak, guides the understanding that metals to the right of Pt strongly bind hydrogen atoms, impeding evolution, while metals to the left weakly bind hydrogen, impeding stabilization and preventing reactions [17].

2.2. Oxygen Evolution Reaction (OER)

The OER is a complex electrochemical multistep four-electron/proton transfer process that occurs at the anode. This process involves breaking H–O bonds and forming O–O bonds and is the main bottleneck for water electrolysis in acid media. Two primary reaction mechanisms have been identified in acidic conditions: the adsorbate evolution mechanism and the lattice-oxygen participation mechanism [11,19].

The adsorbate evolution mechanism involves the conversion of two water molecules adsorbed at the active site into oxygen. Through a series of four consecutive proton-electron transfer events mediated by OH*, O*, and OOH* intermediates, these water molecules lead to O_2 formation. The sequence begins with the adsorption of a water molecule onto the active site and a deprotonation process, forming the OH* intermediate (Equation (16)). Following this, another deprotonation takes place, leading to the conversion of the adsorbed OH* into an oxygen-related intermediate, denoted as O* (Equation (17)). During the nucleophilic attack, another water molecule interacts with the O* intermediate, promoting the generation of an O–O bond and forming the intermediate OOH* (Equation (18)). The final deprotonation process electrocatalyzes the conversion of OOH* into O_2 (Equation (19)), which is then released from the active site, completing the adsorbate evolution mechanism [19,20]. The electrochemical reactions in Equations (16)–(19) represent the whole process just described.

$$H_2O + * \rightarrow OH^* + H^+ + e^- \quad (16)$$

$$OH^* \rightarrow O^* + H^+ + e^- \quad (17)$$

$$O^* + H_2O \rightarrow OOH^* + H^+ + e^- \quad (18)$$

$$OOH^* \rightarrow O_2 + H^+ + e^- \quad (19)$$

Furthermore, the term 'lattice oxygen' refers to oxygen atoms that constitute the crystal lattice structure of the electrode material, likely a metal, involved in the OER process. Lattice oxygen actively participates in the OER mechanism, contributing to the formation of molecular O_2. Researchers have confirmed the involvement of lattice oxygen in the OER process through isotopic labeling and differential electrochemical mass spectrometry [19].

In the lattice-oxygen participation mechanism, the adsorbed H_2O undergoes a transformation into O* after two successive deprotonations, similar to the first two steps of the adsorbate evolution mechanism (Equations (16) and (17)). O* and a lattice oxygen, O_L, then couple to form an O_2 molecule and an oxygen vacancy (Equation (20)). At the beginning of the reaction, O_2 can also be formed directly between lattice oxygen atoms through direct coupling (Equation (21)). The formed oxygen vacancies undergo a refilling process, where oxygen atoms in the water molecules fill the vacancies and undergo a deprotonation process to form adsorbed hydrogen (Equation (22)). The latter is then removed to create a clean active site (Equation (23)) [19,20].

$$O^* + O_L \rightarrow O_2 + V_0 \quad (20)$$

$$2O_L \rightarrow O_2 + 2V_0 \quad (21)$$

$$V_0 + H_2O \rightarrow O_L + H^* + H^+ + e^- \quad (22)$$

$$H^* \rightarrow * + H^+ + e^- \quad (23)$$

The lattice-oxygen participation mechanism exhibits non-concerted proton-electron transfer steps on certain oxides, leading to significant pH dependence [19]. The choice of OER mechanism depends both on the applied electrocatalyst and voltage; at lower voltages, the process undergoes the adsorbate evolution mechanism, while at higher voltages, lattice oxygen is oxidized [11,19].

As shown in Figure 5, OER electrocatalysts are classified into three types: precious metal, non-precious metal, and carbon-based materials. However, efforts to enhance the OER in acidic media have primarily centered around Ir and Ru-based electrocatalysts. Ir-based materials, including iridium oxide (IrO_x) and 0-valent Ir, are benchmarks for their stability and electrocatalytic activity for water oxidation in strongly acidic conditions. Amorphous IrO_x, with its flexible structure and increased electrocatalytic activity compared to crystalline IrO_2, has also been in focus [19].

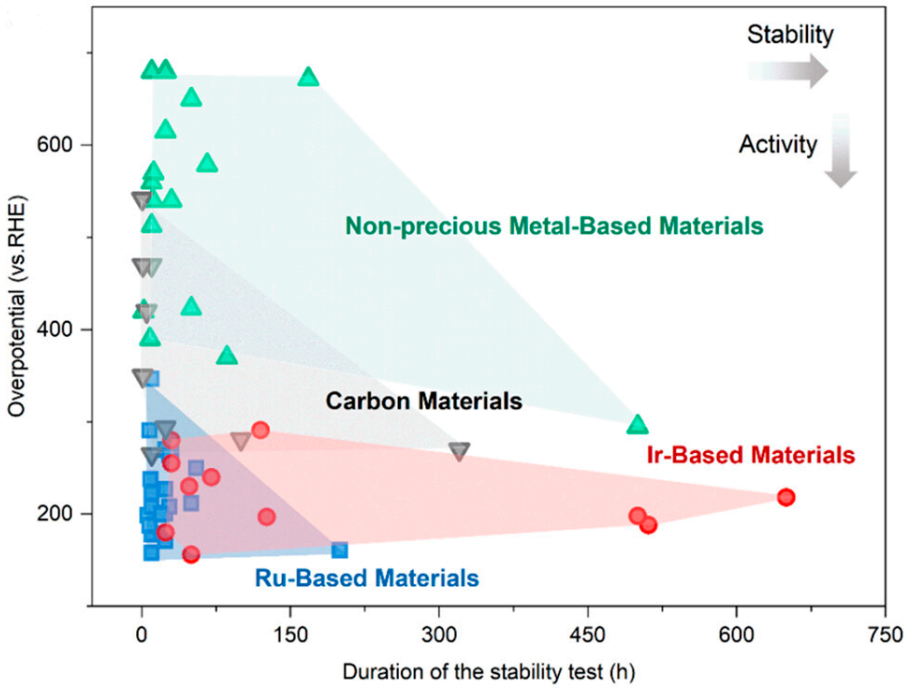

Figure 5. Comparative analysis of overpotential as a function of the stability test time for different electrocatalyst types in recent OER studies [19].

In the pursuit of more economically viable options, Ru-based electrocatalysts have emerged as a promising alternative to Ir-based materials. While Ru-based materials exhibit substantial electrocatalytic activity, stability concerns arise as they tend to dissolve in an acidic OER environment. Apart from this, non-precious metal and carbon-based materials are gaining attention as potential electrocatalysts for the OER in acidic media due to their cost-effectiveness and abundance [19,20]. These materials are alternative options to precious metals like Ir and Ru, addressing the challenges associated with their high cost and scarcity. While non-precious metal and carbon-based electrocatalysts may not always match the activity of precious metals, ongoing research is focused on optimizing their performance through structural modifications, doping, and advanced synthesis techniques.

2.3. Electrochemical Water Splitting Characterization

This section discusses the critical evaluation parameters for electrochemical water splitting. Assessing the effectiveness of this process involves considering various factors such as overpotential at a defined current density, electrochemical surface area (ECSA), Tafel slope, exchange current density, turnover frequency (TOF), faradaic efficiency, as well as mass and specific activities. The Tafel slope and overpotential at a set current density, along with exchange current density and TOF, all provide insights into the kinetic activity (i.e., how fast the reaction proceeds), and these data can be extracted from the electrode polarization curves.

2.3.1. Overpotential

The overpotential, η, is the additional energy input necessary to overcome the intrinsic kinetic barrier in both the HER and the OER. This term directly correlates with a cell's voltage efficiency, indicating that more energy than thermodynamically anticipated is required to drive a reaction in an electrolytic cell [11,12]. Thus, when studying the HER and OER using a working electrode, deviations from the reversible thermodynamic potentials, denoted as overpotentials, are expected and denoted as η_{HER} and η_{OER} (Equations (24) and (25)). These deviations can be determined by the potential difference between the applied potential, denoted here as E_{RHE} (corresponding to the potential mea-

sured versus the reversible hydrogen electrode, RHE, reference), and each half-reaction's thermodynamically determined reduction potential [11,12].

$$\eta_{HER} = E_{RHE} - 0\ V \quad (24)$$

$$\eta_{OER} = E_{RHE} - 1.229\ V \quad (25)$$

In commercial water electrolysis devices, the system operates at a fixed current density and constant cell voltage, ranging from 1.8 V to 2.0 V, depending on the electrocatalyst for HER and OER. The established benchmark for comparing HER and OER electrocatalysts across different pH media is a current density of 10 mA cm^{-2} [11]. There are different types of overpotential in the water-splitting process, including activation, ohmic, concentration, and bubble overpotential.

Activation Overpotential

It is associated with the energy required to initiate and drive a reaction at the electrode-electrolyte interface. Therefore, it encompasses the electrode kinetics involving the charge transfer. The anode activation overpotential (η_a, Equation (26)) and the cathode activation overpotential (η_c, Equation (27)) can be computed using the Tafel equation [11],

$$\eta_a = a_a + b_a \log j \quad (26)$$

$$\eta_c = a_c + b_c \log j \quad (27)$$

where a_a and a_c are the constants of the Tafel equation at the anode and the cathode, respectively; b_a and b_c are the Tafel slopes at the anode and the cathode, respectively, and j is the current density. To achieve higher efficiencies and lower energy consumption of the electrochemical cell, the overpotential can be reduced by choosing an appropriate electrocatalyst for the process.

Ohmic Overpotential

The resistance that the current faces as it passes through the electrodes, electrolyte, and any connections in the system causes an additional voltage drop, resulting in a resistance overpotential. The main resistances that can be found in an electrolyzer are related to the bipolar plates (BPs), the electrode backing layers (EBL), and the membrane (M). Thus, the ohmic overpotential can be expressed by Equation (28),

$$\eta_{ohmic} = \eta^a_{BP} + \eta^c_{BP} + \eta^a_{EBL} + \eta^c_{EBL} + \eta_M \quad (28)$$

where a and c refer to the anode and the cathode side, respectively [11].

Concentration Overpotential

The concentration of reactants or products near the electrode can be significantly depleted due to the consumption or increased due to the generation of species during the electrochemical reaction. This depletion/generation creates a concentration gradient that enables the diffusion of species toward or away from the electrode, as dictated by Fick's law. The concentration overpotential can be interpreted as the resistance to this reactant/product mass transfer, which is more pronounced in higher current densities [11]. Overall, it can be expressed as the sum of the concentration overpotential at the anode and the cathode (Equation (29)).

$$\eta = a + b \log j \quad (29)$$

When an electrochemical reaction occurs at the electrode surface, the reaction rate is often limited by the transport of reactants to the electrode or the removal of products from the electrode. This limitation is particularly pronounced when dealing with electrochemical processes involving gases or species in solution. By agitating the solution, mass transport is

improved, and diffusion limitations are reduced, promoting more effective replenishment of reactants or removal of products near the electrode [11].

Bubble Overpotential

The presence of bubbles directly affects the overall electrolysis process performance. These bubbles can either accumulate on the electrode surface, reducing the effective active area where the reaction takes place, or disperse in the electrolyte. This phenomenon, known as the "bubble effect," leads to an important increase in the overpotential and a significant ohmic voltage drop [11]. According to the Tafel equation, the overpotential is given by Equation (30).

$$\eta = a + b \log j \tag{30}$$

Knowing that the current density is given by j = i/A, where i is the current and A is the surface area of the electrode, j can be expressed in terms of a reduced surface area (i.e., j_θ) by Equation (31),

$$j_\theta = \frac{i}{A(1-\theta)} \tag{31}$$

where θ is the bubble coverage ratio on the electrode. In this case, the Tafel equation can be expressed as Equation (32),

$$\eta = a + b \log\left(\frac{i}{A(1-\theta)}\right) \tag{32}$$

meaning there is an increase in overpotential due to the electrode area occupied by the bubbles being unavailable to catalyze the desired reaction.

2.3.2. Tafel Slope and Exchange Current Density

Tafel slope and exchange current density are key parameters in the electrochemical characterization of systems. These parameters are derived from Tafel plots, which can be obtained through linear scan voltammetry (LSV) at low scan rates or by applying constant potential/current methods. LSV is one of the most used techniques for studying redox reactions involving several charge transfer steps. The experimental setup involves a three-electrode system comprising a working electrode (WE), a counter electrode (CE), and a reference electrode (RE). These electrodes are connected to a potentiostat and immersed in a solution of interest, forming an electrochemical cell. The potentiostat controls the electric potential of the WE with respect to the RE by applying a current flow between the WE and the CE. The potentiostat adapts the current flowing through the cell until the electric potential measured at the WE with respect to the RE (built to have a stable, constant, and well-known potential) is equal to the user-specified input. The current is indirectly measured, effectively quantifying the electrochemical response of the chemical reaction in question, generating a current (i) vs. potential (E) graph [21].

Knowing the electrode's surface area and the electrochemical reaction's overpotential, one can plot the overpotential as a function of the logarithm of the current density, represented as log j. This graphical representation, known as a Tafel plot, is a valuable tool for determining the Tafel slope and the exchange current density. While the Tafel Equation (Equation (30)) is often used to describe the rate of an electrochemical reaction at an electrode (Equations (26) and (27)), the Butler–Volmer Equation (Equation (33)) expresses the relationship between the overpotential and current at the electrical interface [11],

$$j = j_0\left[\exp\left(\alpha_a \frac{n F \eta}{R T}\right) - \exp\left(-\alpha_c \frac{n F \eta}{R T}\right)\right] \tag{33}$$

where j is the current density, j_0 is the exchange current density, n is the number of exchanged electrons, F is Faraday's constant, T is the absolute temperature in Kelvin, α_a and α_c are the charge transfer coefficients for anodic reaction (OER) and cathodic reaction

(HER), respectively, η is the overpotential, and R is the ideal gas constant [11]. The high overpotential approximation on the Butler–Volmer equation can be used to obtain the Tafel Equations for the anodic and cathodic processes. In the high overpotential approach, the reverse reaction can be neglected. For a negative overpotential, Equation (34) can be written.

$$\exp\left(-\alpha_c \frac{n\,F\,\eta}{R\,T}\right) \gg \exp\left(\alpha_a \frac{n\,F\,\eta}{R\,T}\right) \tag{34}$$

Therefore, Equations (35) and (36) can be derived,

$$j_c = j_0 \exp\left(-\alpha_c \frac{n\,F\,\eta}{R\,T}\right) \tag{35}$$

$$\eta = -\frac{R\,T}{\alpha_c\,n\,F} \ln\left(\frac{j_c}{j_0}\right) \tag{36}$$

where the slope for the cathodic polarization can be expressed by $-2.303\frac{R\,T}{\alpha_c\,n\,F}$ if a base 10 logarithm system is used (Equation (37)).

$$\eta = -2.303\frac{R\,T}{\alpha_c\,n\,F} \log\left(\frac{j_c}{j_0}\right) \tag{37}$$

On the other hand, for a positive overpotential, Equation (38) can be written.

$$\exp\left(\alpha_a \frac{n\,F\,\eta}{R\,T}\right) \gg \exp\left(-\alpha_c \frac{n\,F\,\eta}{R\,T}\right) \tag{38}$$

Therefore, Equations (39) and (40) can be derived,

$$j_a = j_0 \exp\left(\alpha_a \frac{n\,F\,\eta}{R\,T}\right) \tag{39}$$

$$\eta = \frac{R\,T}{\alpha_a\,n\,F} \ln\left(\frac{j_a}{j_0}\right) \tag{40}$$

where the slope for the anodic polarization can be expressed by $2.303\frac{R\,T}{\alpha_a\,n\,F}$ if a base 10 logarithm system is applied (Equation (41)).

$$\eta = 2.303\frac{R\,T}{\alpha_a\,n\,F} \log\left(\frac{j_a}{j_0}\right) \tag{41}$$

As shown in Equations (37) and (41), for the anodic and cathodic side reactions, respectively, the charge transfer coefficient (α) and the number of electrons transferred (n) are inversely related to the Tafel slope. A better-performing electrocatalyst possesses a smaller Tafel slope value because it requires less overpotential to attain a higher current density. The Tafel slope value can usually be determined with minimal experimental error when an LSV is acquired at low scan rates. However, when using a high scan rate, larger experimental errors can be present in the determination of j_0 [11]. For electrocatalytic processes, the j_0 is obtained by extrapolating linear fits and extracting the current density at zero overpotential, as shown in Figure 6. The higher the j_0, the better the electrocatalyst [11].

Alternatively, the polarization curves can also be obtained using constant potential/current methods, specifically chronoamperometry/chronopotentiometry, where the current/potential after stabilization is recorded and then plotted as a function of the applied potential/current. Although more time-consuming, these two methods usually lead to more trustworthy data than LSV.

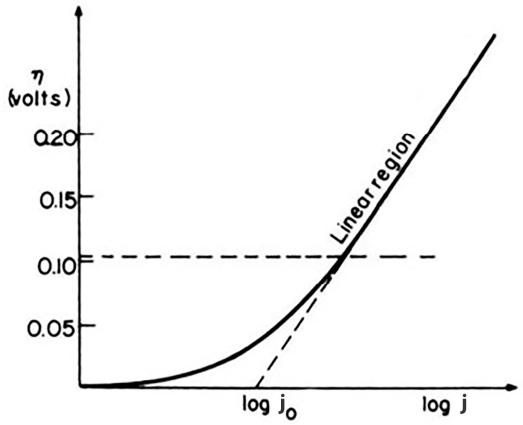

Figure 6. Ideal Tafel plot and exchange current density graphical determination. Adapted from [22] with permission from Springer Nature.

2.3.3. Turnover Frequency

In electrochemistry, turnover frequency (TOF) is a performance metric for electrocatalysts, providing insight into their efficiency. It indicates the rate at which an electrocatalyst can produce products or exhaust reactants with a fixed quantity of electrocatalyst in a specified amount of time. For instance, it determines how much gas, either H_2 or O_2, is produced at each electrocatalyst active site. Regarding reactions like HER or OER, TOF values help us understand how quickly these processes happen. TOF is not determined by the amount of electrocatalyst present in the reaction but by how well the electrocatalyst is dispersed to cover a specific area. Scientific evidence has proven that when the coverage falls below 100%, TOF exhibits a linear behavior [11,23]. TOF can be computed using Equation (42),

$$\mathrm{TOF} = \frac{\mathrm{j}\,\mathrm{N_A}}{\mathrm{n}\,\mathrm{F}\,\Gamma} \tag{42}$$

where j is the current density, n is the number of transferred electrons (2 e^- for HER and 4 e^- for OER), N_A is the Avogadro number, and Γ is the surface concentration of active sites of the electrocatalyst [11]. The higher the TOF, the better the electrocatalyst.

2.3.4. Faradaic Efficiency

Faradaic efficiency (FE or η_{Faradaic}) is a crucial parameter in electrochemistry. It measures how effectively charge (electrons) is transferred in an electrochemical system, i.e., how much of the measured current is attributed to the desired reactive process, excluding contributions from secondary processes such as capacitive effects or undesired Faradaic reactions. FE can be defined as the ratio of the actual amount of the collected product to the theoretical amount that could be generated from the total charge passed during the process (Equation (43)) [11,24]. It can be determined using gas chromatography for both HER and OER [11].

$$\eta_{\mathrm{Faradaic}} = \frac{\mathrm{V_{H_2/O_2}\ (produced)}}{\mathrm{V_{H_2/O_2}\ (calculated)}} \tag{43}$$

Determining FE for OER can also be performed using rotating ring disk electrode (RRDE) measurements. The RRDE data enables using Equation (44) to calculate the FE of the process under study,

$$\mathrm{FE} = \mathrm{j_R}\frac{\mathrm{n_D}}{\mathrm{j_D}\,\mathrm{n_R}\,\mathrm{N_{CL}}} \tag{44}$$

where j_R is the ring current density, n_D is the number of electrons transferred at the disk electrode, j_D is the disk current density, n_R is the theoretical number of electrons transferred during OER (4 e^-), and N_{CL} is the collection efficiency, defined as the fraction of the species generated at the disk that is detected at the ring electrode [11].

3. Proton-Exchange Membrane Electrolysis

Currently, there are two commercially available types of electrolyzers: the alkaline water electrolyzer (AWE) and PEMEL. However, promising technological advancements have led to the development of two other types of electrolyzer: the anion-exchange membrane electrolyzer (AEMEL) and the solid oxide electrolysis cell (SOEC). These technologies are under development and can potentially represent a significant step forward in the field [4]. Table 1 briefly compares the four electrolyzer technologies in terms of the used electrolyte, the operating current density, the stack lifetime, and the typical temperature range.

According to the IEA, the global installed capacity of water electrolysis for H_2 production reached around 300 MW by the end of 2020. AWE was the most widely used technology, accounting for 61% of the total installed capacity, while PEMEL accounted for 31%. The remaining capacity was attributed to unspecified electrolyzer technologies and SOECs [4,25,26]. Figure 7 provides a simplified schematic representation of the components and processes occurring in AWE and proton-exchange membrane (PEM) electrolysis.

Table 1. Comparison between the available electrolyzer technologies [27].

	PEMEL	AWE	SOEC	AEMEL
Electrolyte	Solid (proton-exchange membrane)	Liquid (20–30 wt.% KOH)	Solid (ceramic)	Solid (anion-exchange membrane)
Current density (A/cm^2)	0.2–4	0.4–1	0.5–1.5	0.2–2
Stack lifetime (full load hours)	60,000–90,000	60,000–100,000	20,000–50,000	5000–40,000
Operating temperature range (°C)	50–80	70–90	500–900	40–80

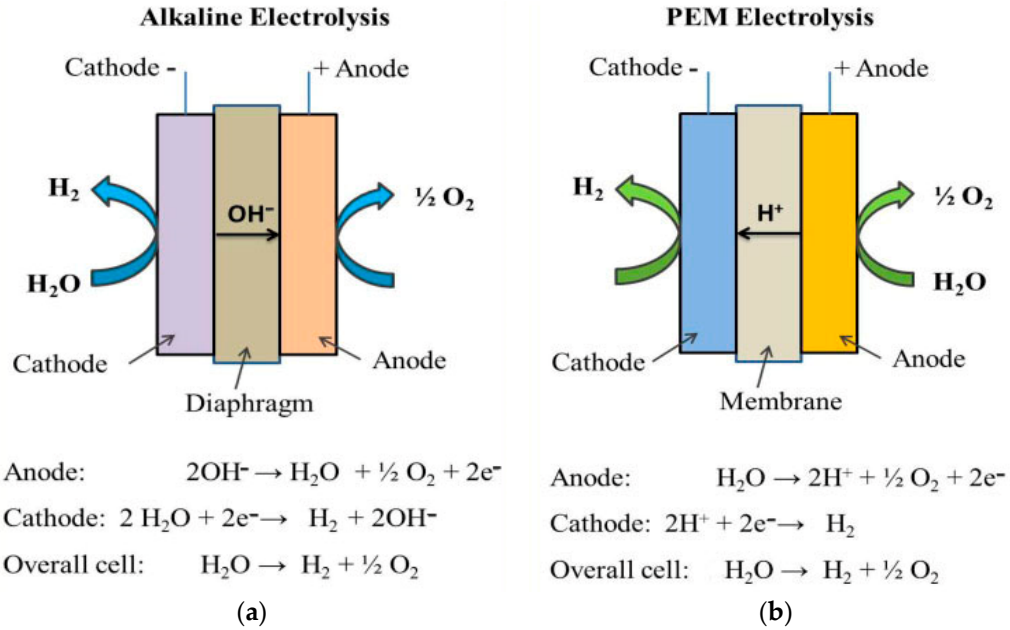

Figure 7. Schematic representation of (**a**) AWE and (**b**) PEM electrolysis (adapted from [28]).

The installed capacity of electrolyzers for H_2 production is expected to experience significant growth in the coming years. According to industry projections, the global installed electrolyzer capacity could reach up to 54 GW by 2030, considering the capacity under construction and planning. Moreover, if all projects at early planning stages are included, the capacity could increase to as much as 91 GW by 2030 [4,25]. The present work focuses on PEMEL, which is currently the most advanced commercial technology.

3.1. PEMEL Working Principle

When a direct current passes through the electrodes, the anode becomes positively charged, and the cathode becomes negatively charged. At the anode, water is oxidized to form O_2 gas and protons (H^+). The protons produced at the anode migrate through the PEM to the cathode, where they combine with electrons (e^-) produced in the water oxidation process to form H_2 gas. An external power supply acts as the driving force for these two processes. The H_2 and O_2 gases produced at the electrodes are then collected and separated for use [28].

Commercial PEMEL offers technical aspects such as efficiency of 50–83%, operating temperature between 50 and 80 °C, higher current densities in a range of 1–2 A/cm^2, and production capacities between 0.2–60 Nm^3/h. Compared to AWE, PEMEL produces significantly higher purity (99.999%) H_2 [7,29]. PEMEL has overcome some AWE drawbacks, such as the overall system efficiency, current density, and the purity of produced H_2. However, one of the key obstacles in developing PEMEL is the significant cost associated with the various components, such as the electrode materials, current collectors, bipolar plates, and membranes [4,30].

3.2. PEMEL Components

A PEMEL device comprises several components in each cell, including an electrolyte membrane, electrodes, bipolar plates (BPs), porous transport layers (PTL), current collectors, and gaskets. Figure 8 presents a schematic representation of the main components of a PEMEL cell.

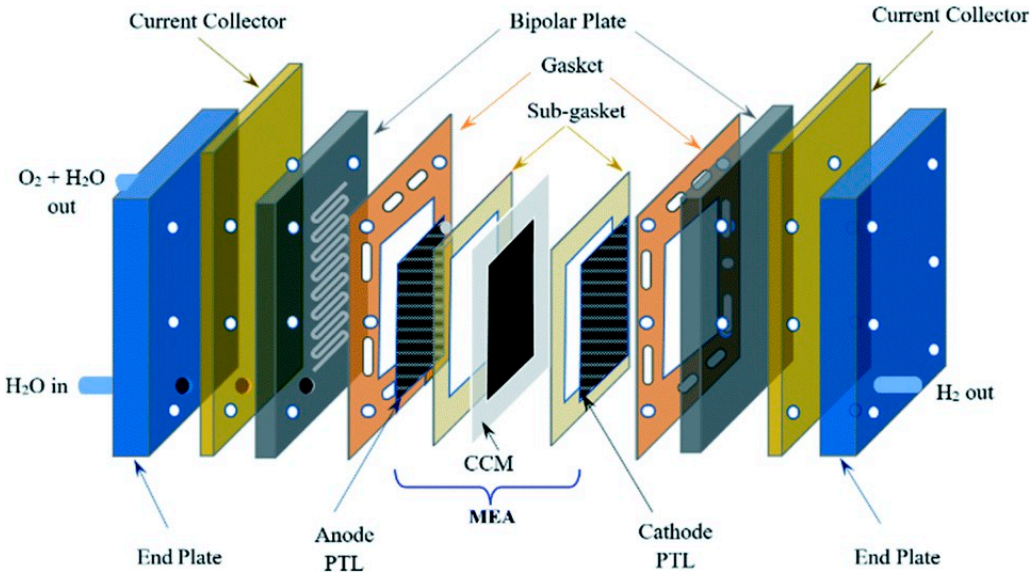

Figure 8. Schematic representation of the main PEM electrolysis cell components [31]. Reprinted with permission from the Royal Society of Chemistry.

The membrane is made of a solid polymer electrolyte film, typically a perfluorinated compound known as Nafion, with a thickness of around 50–175 µm. It selectively allows H^+ protons to flow and physically separates the anode and cathode compartments of the cell, avoiding the mixing of oxygen and hydrogen gases [32]. The membrane-electrode assembly (MEA) basically refers to the membrane sandwiched between anode and cathode. Specifically, the PEM's edge is protected by sub-gaskets and sandwiched by an electrocatalyst layer and a PTL on each side. The central layer of the MEA is the polymer electrolyte membrane. On either side of the membrane, there is the electrocatalyst layer, each requiring a different electrocatalyst for the anode and cathode reactions [33]. An iridium oxide (IrO_2) electrocatalyst layer is typically deposited on the anode, where the OER occurs. A Pt electrocatalyst layer is deposited on the cathode side, where the HER occurs.

The PTL, also called the gas diffusion layer, is a "multi-purpose" component, enabling efficient mass transport of reactant and product gases, managing water within the electrolyzer to prevent blockages, maintaining optimal pressure and gas distribution, and providing mechanical support for the MEA. It is typically composed of an electrically conductive porous material like titanium. The PTL on the cathode side needs to manage the flow of the produced H_2 gas bubbles. On the anode side, it allows the flow of liquid water to electrocatalytic sites while expelling O_2 gas bubbles that could obstruct the anodic process. PTL enhancements are focused on the anode side mainly due to two reasons: (i) ineffective water management enhances mass transport overpotentials (leading to lower efficiencies) and can eventually cause cell failure, and (ii) the high oxidation potential applied at the anode side can cause the PTLs to corrode, further diminishing efficiency and increasing costs. The PTL's porous structure also ensures uniform gas distribution, critical for preventing localized pressure variations during electrolysis [34].

The main responsibility of the BPs in electrolyzers is to conduct electricity, serving as pathways for the flow of electrical current between adjacent electrolysis cells. Additionally, the BPs allow gas flow through "channels" on their surfaces, directing H_2 and O_2 gases away from the electrodes to collection and evacuation points. To enhance efficiency, BPs should have low electrical resistance, often achieved using materials with good electronic conductivity, such as certain metals or carbon composites [28,35].

Finally, the primary responsibility of the current collector is to allow electric conduction between the electrode and the BPs while also ensuring efficient gas transport from the electrode to the flow channels [28,36]. This component completes the electrical circuit between the anode and cathode, enabling a continuous flow of electrons to sustain the electrolysis process. BPs are typically Ti-based, largely contributing to the final stack cost. This is mainly due to the high corrosion resistance of Ti, making it a good candidate to withstand highly adverse operating conditions, as well as good conductivity [37,38]. However, alternatives are being reported in the literature: Nb,Ti-coated stainless steel plates that possess improved electric conductivity and lower cost [39]; Ta, W, Mo, Nb, AISI 316 L, and AISI 304 L pristine plates that, albeit ineffective on their own due to inadequate corrosion resistance or increasing interfacial contact resistance due to the formation of non-conducting surface oxides, could serve as substrates to produce coated BPs with interesting properties [37]; and Ti-coated stainless steel substrates (AISI 321, AISI 316 L, and AISI 904 L) [38].

3.3. PEMEL Systems

In large-scale facilities, a more detailed subsystem is required to operate each technology successfully. These subsystems, also known as Balance of Plant (BoP), are essential for the optimal functioning of the main unit and involve a series of different equipment, depending on the technology used. The BoP of H_2 systems includes subsystems such as water treatment, power supply, heat exchangers, cooling systems, piping, instrumentation, and control systems [4,7].

The process begins by introducing deionized water into the O_2 separator. To ensure that the system remains unharmed, the water conductivity must be kept below 0.1 μS/cm [40]. The water is transported to the electrolyzer stack, the system's most critical part. Before entering the electrolyzer stack, an ion exchange resin cartridge is employed to ensure low water conductivity. The unreacted water and produced O_2 are emitted from the stack at the anode outlet and sent back to the O_2 separator. The temperature inside the system is regulated by a heat exchanger and is typically kept between 60 and 80 °C. It is important to mention that if the produced O_2 is not required for another process, it is usually released into the atmosphere. Otherwise, it is subjected to drying and purification treatments. Only the anode side of the system is responsible for circulating water [4,40]. Figure 9 presents a chart of the production process flow using a PEMEL system.

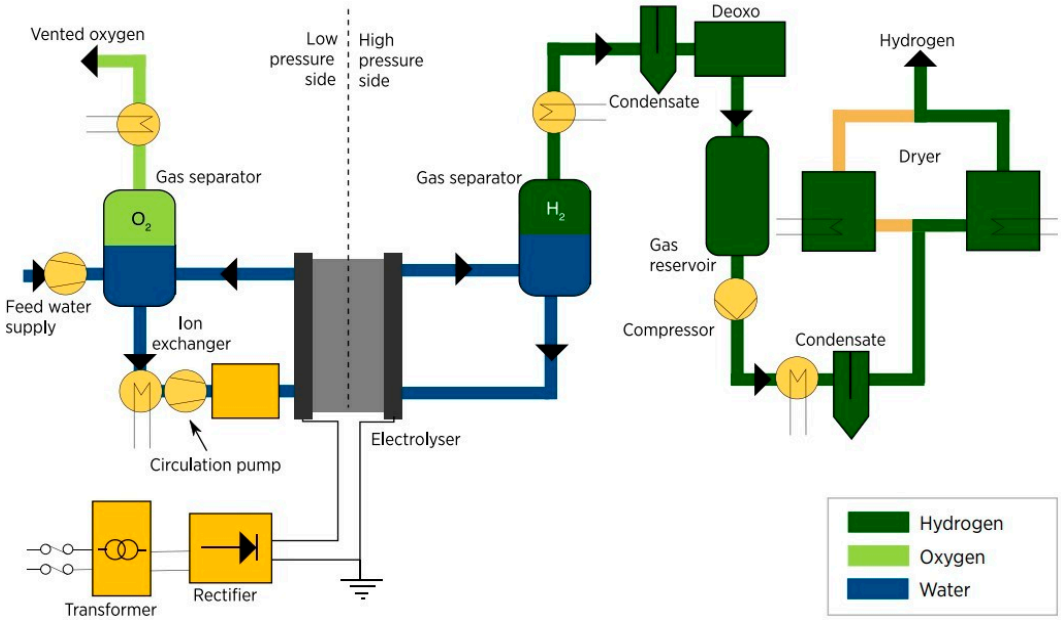

Figure 9. H_2 production process flow chart by PEM electrolysis [7].

On the other side, i.e., the cathodic side, H_2 and water are released as a gas mixture and then cooled to be separated at the H_2 separator. Water is returned to the O_2 separator. The H_2 is then purified to reduce both O_2 and water concentration below 5 ppm by using a catalytic deoxo purification device and an adsorptive dryer, respectively, before being stored. While the cathodic side maintains a pressure of up to 30 bar, the O_2 side is typically kept at ambient pressure to simplify system design and minimize cross-permeation [4,40]. In addition, power and control electronics and safety equipment are also included in the system.

3.4. PEMEL Costs

According to The Oxford Institute for Energy Studies, the second most significant cost factor in the production of green H_2 is the electrolysis system, making up approximately 15% of the total cost share [41]. Despite the availability of commercially viable PEM electrolyzers, this technology is currently considered expensive in terms of both Capital Expenditures (CAPEX) and operational expenditures (OPEX). Nevertheless, it is anticipated that the cost of this technology will decrease significantly over time as H_2 production through electrolysis continues to grow and global policies focus on decarbonizing various sectors by using H_2.

PEMEL System Cost Breakdown

As previously stated, an electrolysis system primarily comprises an electrolyzer stack and the various components that allow the unit to function optimally, namely the BoP. According to IRENA, the PEM electrolyzer stack accounts for roughly 45% of the total cost of the electrolysis system, while the BoP accounts for the remaining 55% [7]. This share, however, is highly dependent on each manufacturing strategy, business case, design, and technical specifications. Figure 10 provides the cost breakdown for the different components of a 1 MW PEM electrolyzer.

The cost components of PEMEL stacks are primarily driven by the BPs, which account for approximately 56% of the total share of the stack. The other major component on the stack is the MEA, accounting for 24% of the total cost. This high cost is primarily due to the materials used during the MEA manufacturing process, which include rare and expensive materials such as Ir or Pt. This highlights the need to improve the cost-effectiveness of PEMEL stacks. Strategies that could be implemented to address this issue include reducing

the membrane thickness, avoiding expensive electrocatalysts and coatings, and redesigning the PTLs and BPs [7].

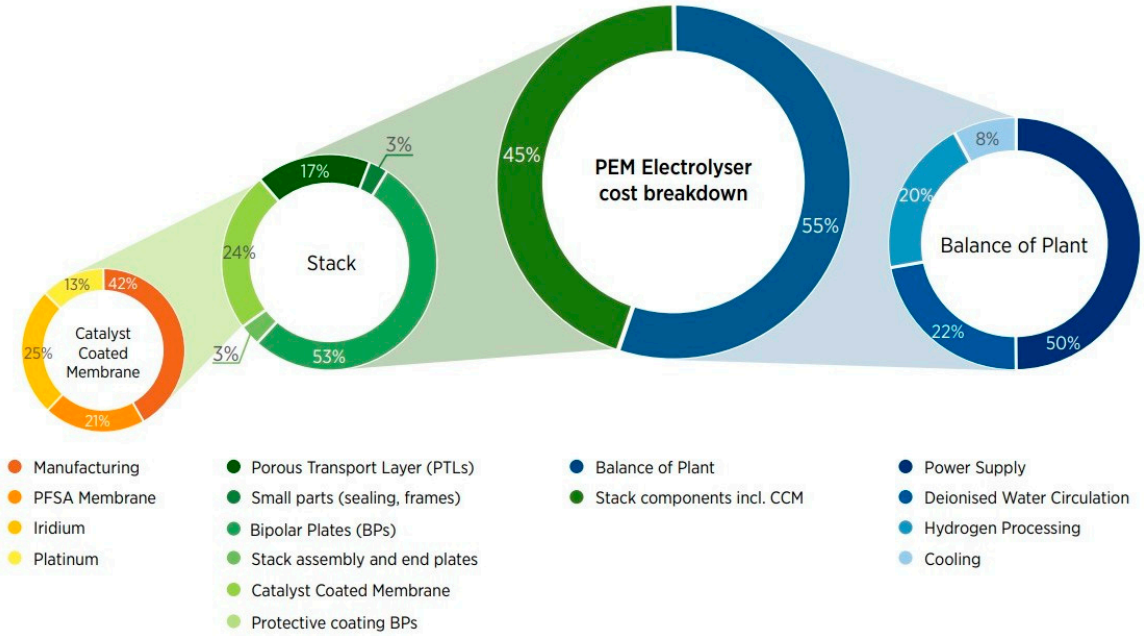

Figure 10. Cost components for a 1 MW PEM electrolysis system, from full system to stack and BoP components [7].

On the other hand, the BoP main cost is the power supply, accounting for 50% of the total. This is followed by the water circulation system and the H_2 drying and purification treatments, with 22% and 20% of the total cost, respectively. Extending initiatives beyond the 1 MW threshold is critical for lowering costs associated with plant balance in green H_2 production. The findings of IRENA's Green Hydrogen Cost Reduction report emphasize the efficiency gains that result from scaling up electrolyzer modules. For example, a 100 MW electrolyzer module can achieve nearly a 50% reduction in operational costs compared to a smaller 5 MW module [7].

Finally, reducing the content of PGMs, particularly high-cost elements such as Pt and Ir, is a critical area for innovation. Given their significant contribution to overall system costs, R&D efforts should be directed toward developing alternative materials, thin films, and components that can effectively replace or reduce reliance on these expensive PGMs.

3.5. PEMEL Manufacturers

According to "Global Market Insights", the global market size of PEM electrolyzers was valued at 1.7 billion USD in 2022 and is anticipated to grow at a compound annual growth rate (CAGR) of 24.1% between 2023 and 2032, reaching 55.8 billion USD [42]. In the upcoming years, it is expected that the market for PEM electrolyzers will expand due to rising demand for H_2 as a clean energy carrier and advancements in technology that make PEM electrolyzers more efficient and affordable. Additionally, PEM electrolyzer technology advancements have improved performance, reduced costs, and raised efficiency, making them a potential viable option for commercial and industrial uses. This includes better system integration, enhanced membrane durability, and the development of cost-effective electrocatalysts. However, market growth is expected to be restricted by high initial costs, limited infrastructure, reliance on RES, and other electrolysis technologies, such as AWE and SOECs [43].

Table 2 lists the key industry players and their PEMEL system specifications, which are crucial to evaluating the overall performance and potential of specific applications. It is

intended to provide an overview of the relevant details of some currently available PEMEL systems on the market.

Table 2. Specifications of commercially available PEM electrolysis systems.

Key PEM Electrolyzer Manufacturers									
Company	**HQ**	**Product Name**	**H_2 Flow (Nm^3/h)**	**O_2 Flow * (Nm^3/h)**	**System Efficiency (kWh/kg)**	**Equivalent Power Rating (MW)**	**Operating Pressure (bar)**	**Water Consumption (L/kg_{H2})**	**Hydrogen Purity (%)**
Nel Hydrogen [44]	Norway	M Series	2020	4040	51.2	10	30	10	+99%
H-TEC Systems [45]	Germany	MHP	213–2130	106.5–1065	51	10	30	1850 kg/h	99.97–99.9999
Siemens Energy [46]	Germany	Sylizer 300	100–22,251 **	50–11,075	N/A	N/A	8.7–17.5	10	99.9995
Cummins Inc [47]	USA	HyLYZER series	200–4000	100–2000	51	1–20	30	9	99.99–99.998
SinoHy Energy [48]	China	HGPS-50 HPGS-200	50–200	25–100	N/A	0.25–1	32	N/A	99.999
Plug Power Inc [49,50]	USA	EX-2125D EX-4250D	990–1989	495–994.5	49.9	0–10	40	10.23	99.999
Elogen [51]	France	Multi MW	Min 2000	Min 1000	48	50.6	30	<2 L/Nm^3 H_2	99.9–99.999

N/A: Not available. * O_2 flow is calculated using the stoichiometric relation 1:2 for O_2 and H_2, respectively. ** Max H_2 flow for Sylizer 300 is 2000 kg/h by using the H_2 conversion data, 1 kg of H_2 = 0.08988 Nm^3 H_2 gas [52].

Key Performance Indicators (KPIs) play a crucial role in the development process as they provide a quantitative and measurable way to assess and optimize the performance of any available technology. Table 3 presents the KPIs defined by IRENA for PEM electrolyzers. According to the table, several key strategies on the R&D side can significantly advance PEM electrolyzer development. These include reducing membrane thickness, reducing electrocatalyst quantities by reengineering electrode concepts, removing expensive coatings, redesigning the PTLs and BPs, and exploring novel concepts for electrocatalyst recombination.

Table 3. KPI targets for PEM electrolyzer stacks [7].

Parameter	**Unit**	**2020**	**2050**	**R&D Focus**
Nominal current density	A/cm^2	1–2	4–6	Design and membrane
Voltage range	V	1.4–2.5	<1.7	Electrocatalyst and membrane
Operating temperature	°C	50–80	80	Effect on durability
Cell pressure	bar	<30	>70	Membrane, reconversion catalyst
H_2 purity	%	99.9–99.9999	same	Membrane
Voltage efficiency (LHV)	%	60–68	>80	Electrocatalyst
Electrical efficiency (stack)	kWh/kg_{H2}	47–66	<42	Catalyst/membrane
Electrical efficiency (system)	kWh/kg_{H2}	50–83	<45	Balance of plant (BoP)
Lifetime	h	50,000–80,000	100,000–120,000	Membrane, electrocatalyst, and PTLs
Stack unit size	MW	1	10	MEA, PTL

4. Role of the Electrocatalyst

Electrocatalysts play an important role in the water electrolysis process, helping to overcome the inherent thermodynamic challenges of splitting water into H_2 and O_2 gases. The thermodynamic feasibility of this reaction is limited by the need for larger potentials, known as overpotentials, that move the reaction forward. In this situation, electrocatalysis facilitates electrochemical reactions along pathways with lower activation barriers, thereby speeding up the entire process. Electrocatalysts for water electrolysis are heterogeneous

because the electrocatalyst and the reactant are in different phases: the electrocatalyst is solid, while the reactant is liquid [53].

As mentioned, the water-splitting process is thermodynamically unfavorable at STP. It requires an excess of energy to overcome the different overpotentials that primarily arise due to kinetic activation barriers between the initial and final equilibrium states of water molecules during their decomposition. Figure 11 represents the role of the electrocatalyst in the water-splitting process. It shows that the red pathway requires a higher energy input to overcome the kinetic barrier for water electrolysis. Thus, low electrocatalyst activity leads to an increased energy demand for the electrochemical process and, consequently, a lower reaction rate. In contrast, considering the green pathway, significantly less energy is required to overcome the kinetic barriers of the reaction. In this scenario, a more active electrocatalyst corresponds to a reduced energy requirement for the reaction, resulting in a faster reaction rate at lower potentials.

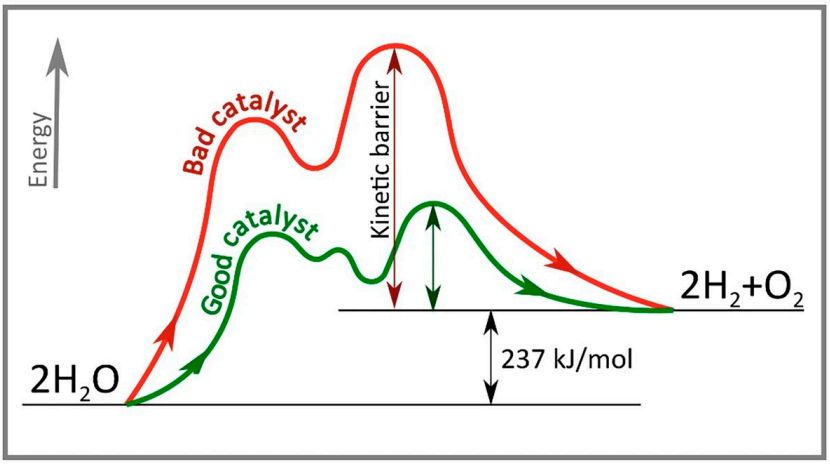

Figure 11. Schematic representation of the role of electrocatalysts in water electrolysis [53]. Reprinted with permission from Springer Nature.

The IRENA report on green H_2 cost reduction highlights that one of the main issues PEM electrolyzers face is their reliance on critical materials, specifically Ir and Pt. The anode side of PEM electrolyzers operates at high potentials (>1.4 V), making it difficult to find materials with long-term operational stability. Iridium, although expensive and scarce, is currently the benchmark material for this purpose. On the other hand, the cathode side requires a material with exceptional electrocatalytic activity for the HER, as is the case of Pt. Additionally, PEM electrolyzers require a substantial amount of materials with high electronic conductivity and mechanical strength. Consequently, some of their components rely on titanium metal (e.g., the PTLs) [7].

The Pt and Ir content in PEM electrolyzers is typically 1 g/kW and 1–2.5 g/kW, respectively. According to IRENA, the existing loading of scarce materials is a barrier to electrolyzer cost and scaling capacity. Only an estimated 3–7.5 GW of annual manufacturing capacity can be supported by the current Pt and Ir production for PEM electrolyzers. However, this is significantly less than the projected manufacturing requirement of 100 GW by 2030 [7]. To overcome one of the limitations on cost reduction and scaling up capacity, the US Department of Energy (DOE) has set the following targets on PGM content for PEM electrolyzers (Table 4). Thus, a reduction of approximately 85% is expected for 2026, and a 96% reduction is expected for 2030. This underscores the immediate need for research, innovation, and industrial efforts to minimize PGM usage (specifically, Pt and Ir) in PEM electrolyzers, ensuring the long-term viability and scalability of green H_2 technologies.

Table 4. DOE targets for PEM electrolyzer PGM content reduction [54].

Characteristic	Unit	2022 Status	2026 Target	Ultimate Target
Total PGM content	mg/cm^2	3	0.5	0.125
(both electrodes combined)	g/kW	0.8	0.1	0.03

4.1. Electrocatalysts for HER

HER electrocatalysts are commonly classified into three main categories: PGM-based, transition metal (TM)-based, and metal-free electrocatalysts [55]. Each category includes a diverse range of materials and strategies, presenting unique advantages and challenges. PGM-based electrocatalysts, such as Pt, have long been considered benchmark materials for HER due to their exceptional activity. However, their scarcity and high cost limit their practical application on a large scale. TM-based electrocatalysts, on the other hand, utilize abundant transition metals to achieve efficient HER electrocatalysis. These electrocatalysts provide a cost-effective alternative, and recent advances have demonstrated their considerable potential. Furthermore, metal-free electrocatalysts have emerged as a promising option, offering low cost and the absence of critical raw materials. Figure 12 presents a graphical compilation of the electrocatalysts typically studied for the HER. The following sub-sections provide an overview of recent advancements in developing cost-effective electrocatalysts for the HER, examining their classification, specific characteristics, strengths, and limitations.

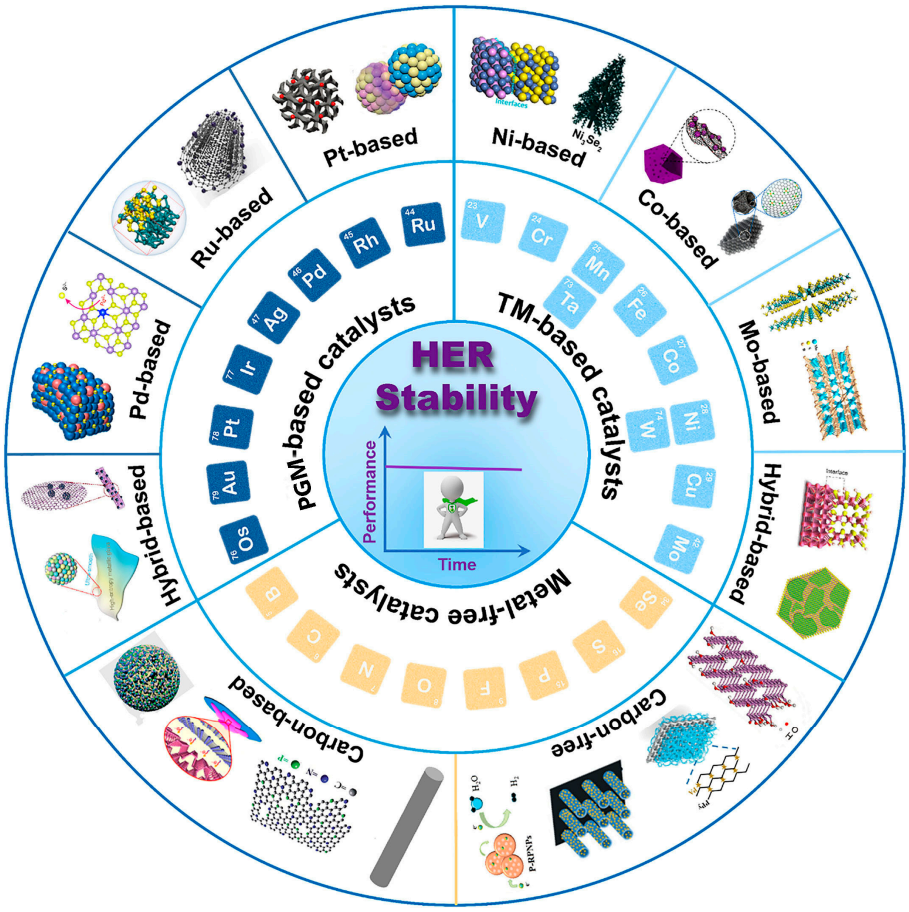

Figure 12. Typical electrocatalysts used for HER [55].

4.2. PGM-Based Electrocatalysts

Pt, Pd, and Ru-based electrocatalysts are commonly used in water electrolysis due to their excellent electrocatalytic performance for the HER; they have the most suitable free

energy of hydrogen adsorption, close to zero [55]. The high cost and low availability of these metals are their main drawbacks. To overcome this, several design strategies for PGM-based electrocatalysts have been proposed. Researchers are working on engineering these electrocatalysts at the atomic and nanoscale levels to enhance their activity and efficiency. This involves optimizing the electrocatalyst's composition, structure, and morphology to improve its performance while reducing the noble metal loading [12,55].

One approach is alloying noble metals with other less-expensive transition metals or creating core–shell structures. Combining noble metals with more abundant and cost-effective materials reduces the overall electrocatalyst cost while maintaining or enhancing electrocatalytic activity. One of the key modifications brought by alloying is the modification of adsorption energies through shifts in the D-band center energy [56]. Examples include, but are not limited to, alloys of Pt with Ti, Co, and Cu [57–60]. A different approach involves designing electrocatalysts with well-defined nanostructures that can significantly improve their electrocatalytic properties. Strategies such as controlling particle size [61], shape [62], and surface structure can enhance the surface area and expose more active sites, leading to improved HER performance. Electrocatalyst support materials are also being explored to increase electrocatalyst dispersion and reduce the noble metal content required for the HER. Carbon-based materials, metal oxides, and other 2D materials, such as graphene, have shown promising results [56,63,64]. Another effective strategy to decrease the amount of Pt is by doping the electrocatalyst surface with lower-cost metal components [12].

4.3. Transition Metal (TM)-Based Electrocatalysts

TM-based materials hold impressive potential but focus mainly on the water-splitting processes in alkaline electrolytes. Earth-abundant TMs (e.g., Ni, Co, W, Fe) have exhibited excellent performance for the HER. Notably, TMs, TM alloys, and transition metal chalcogenides all exhibit outstanding electrocatalytic activities. Ni is the most intensively researched TM, and miscellaneous approaches have been used to achieve the desirable Ni-based electrocatalysts. Alloying is claimed to be a sagacious way to improve the electrocatalytic activity and longevity of TMs. TM alloying can raise electrocatalytic efficiency through a synergistic combination of electrocatalytic metals or by increasing the real and geometric surface area ratio [65]. Oxygen vacancy engineering is an efficient method to simultaneously modulate the electronic structure, conductivity, and the reactive species' adsorption energy. In particular, increasing the oxygen vacancy concentration would decrease the adsorption and dissociation energy of water molecules on electrocatalyst surfaces, thus improving the electrocatalytic activity for alkaline HER. Doping is a conventional strategy to improve the activity of electrocatalysts by increasing active sites, optimizing the electronic structure, inducing phase transformation, and regulating the reaction energy barrier. This strategy is commonly applied, for example, in chalcogenides [65,66]. Further strategies include defect engineering, phase control, and composite engineering, used to produce, for example, Co-based electrocatalysts of the type Co_xA_y (A = P, S, Se), active towards HER in acid media [67]. CoP_x sheets have also been utilized as supports for MoS_2 quantum dots for HER in acid media [68]. These electrocatalysts will not be covered in depth herein as they are more promising for AWE.

4.4. Metal-Free Based Electrocatalysts

Recent advancements in carbon nanomaterials, including graphene, carbon nanotubes (CNTs), graphitic carbon nitride (g-C_3N_4), and three-dimensional (3D) carbon architectures, present exciting possibilities for the development of metal-free electrocatalysts. These materials possess a range of advantages, such as high electronic conductivity, structure tunability at the atomic level, high selectivity, and strong tolerance to acidic/alkaline conditions [69]. Several studies have demonstrated the exceptional electrocatalytic capabilities of metal-free carbon-based electrocatalysts and their unique property of modifying the electrocatalytic performance by manipulating factors such as nanoparticle size, macrostructure, and electrode architecture [69].

CNTs are nanoscale tubular structures belonging to the fullerene carbon allotrope class. However, they can be visualized as the result of rolling graphene sheets. The two types of CNTs can be interpreted using this thought process: single-walled carbon nanotubes (SWCNTs) would consist of a single rolled graphene sheet, and multi-walled carbon nanotubes (MWCNTs) would have concentric graphene sheets rolled around a core SWCNT. CNTs have diameters ranging from a few angstroms to tens of nanometers and can have lengths up to several centimeters. The hollow geometry and conjugated structure of CNTs give rise to outstanding electrical, mechanical, and thermal properties that are not found in other carbon-based materials. The behavior of CNTs can be either semiconducting or metallic, depending on the diameter and arrangement of graphitic rings in their walls. Additionally, CNTs possess a high surface area, with theoretical surface areas of SWCNTs reaching 1315 m^2/g [69,70].

Graphene consists of a one-atom-thick planar sheet of carbon atoms arranged in a honeycomb pattern. It shares several properties with CNTs. For instance, graphene exhibits a large specific surface area of up to 2630 m^2/g, high thermal conductivity (around 5000 W m^{-1} K^{-1} for a single layer), high mechanical strength, good electronic conductivity, and excellent charge mobility (200,000 cm^2 V^{-1} s^{-1}) [69]. Graphene has various physical and chemical properties better than CNTs, making it an attractive material for a wide range of potential applications.

Doping can be used to adjust the properties of carbon by introducing different atoms into its structure [70]. These atoms, such as nitrogen, boron, oxygen, phosphorus, sulfur, chlorine, selenium, bromine, and iodine, are known as dopants. Among these, nitrogen is considered the most effective in enhancing carbon activity. Many studies have shown that nitrogen doping can improve the activity of the OER and HER [70]. Doping carbon with different atoms, like nitrogen or boron, has important effects on activating carbon's properties. It breaks the balance of electrons and spins in the carbon structure, redistributing charges and spins, allowing an effective electron transfer. One example is g-C_3N_4 with nitrogen-doped graphene (N-graphene). g-C_3N_4@N-graphene hybrid possesses a unique molecular structure and electronic properties for electrocatalytic HER application. This metal-free hybrid shows comparable electrocatalytic HER activity with existing well-developed metallic electrocatalysts, such as nanostructured MoS materials. However, its activity is not as high as that of the state-of-the-art Pt electrocatalyst. N-graphene facilitates the electron-transfer process for proton reduction. The findings provide clear evidence that similar to noble metals, the well-designed metal-free counterparts also have great potential for efficient electrocatalytic HER, thus opening a new avenue toward replacing noble metals with broader alternatives in various applications [55,69,70].

4.5. Strategies to Minimize PGM Content

One of the main priorities in solving the critical problem HER faces is lowering the price associated with the amount of Pt needed as an electrocatalyst to enhance the reaction rates. To achieve this, Pt mass activity, i.e., the electrocatalytic current per unit mass of Pt, must be significantly increased. Due to the well-established relationship between mass activity and the quantity of exposed active sites, extensive research has been conducted to reduce the size of Pt-based nanoparticles to clusters or even single atoms [71]. As such, researchers try to increase the surface/volume ratio to obtain a higher amount of isolated Pt sites that can interact with hydrogen ions. This not only enhances HER activity but also improves atom utilization efficiency [72].

However, maintaining the stability of downsized Pt-based nanoparticles remains challenging due to issues like nanoparticle aggregation under a certain temperature and insufficient durability under specific voltages. To overcome these challenges, several strategies are being approached. These include electrocatalyst engineering (designing electrocatalysts with nanoscale structures to increase their surface area and improve electrocatalytic activity or alloying PGMs with other less expensive metals to create electrocatalysts with comparable or improved performance) and surface modification (modifying the surface of PGM

electrocatalysts with other materials or functional groups to enhance their electrocatalytic activity) [72].

Ultralow Pt loading electrocatalysts are an interesting development in this area. These electrocatalysts, consisting of Pt atoms dispersed on supports, significantly reduce the amount of Pt required while retaining high electrocatalytic activity. These electrocatalysts typically have Pt loadings below 10 wt.% and sizes less than 5 nm, with support from materials like carbon ensuring stability and dispersion [72–74]. Another approach is Pt-based alloys, where Pt is mixed with non-noble metals like Cu or Co [57–60]. These alloys often exhibit enhanced electrocatalytic activity, increased durability, and reduced cost. Pt-Ni and Pt-Co alloys are commonly used in fuel cells and other electrochemical devices [72].

5. Future Perspectives

Looking ahead to the future of PEM electrolysis for green hydrogen production, several advancements and considerations are critical for scaling up processes, optimizing parameters, and developing more efficient, cost-effective catalysts.

One key focus is refining the catalyst screening process, where emerging technologies, such as artificial intelligence (AI) and machine learning, hold significant promise. AI-driven modeling and predictive algorithms can accelerate the discovery of high-performance, low-cost catalysts by processing large datasets, including the electrochemical properties of metals, to identify materials with optimal activity, durability, and cost-effectiveness.

Additionally, scaling up PEM electrolyzers requires addressing system efficiency, durability, and cost challenges. Accordingly, parameters like temperature, pressure, and electrode design must be fine-tuned for larger-scale applications. Advanced manufacturing techniques, such as atomic layer deposition, electrodeposition, additive manufacturing, and high-throughput experimentation, may further support the transition to commercial-scale systems.

Innovative water electrolysis systems, such as the semi-vapor approach, are also under development [75]. This system, a proof of concept, employs water vapor at the anode and deionized water at the cathode. It has been demonstrated as a highly energy-efficient and groundbreaking method for performing water electrolysis. By using water vapor at the anode, the process eliminates the need for water pre-treatment, making the technology more cost-effective. This also enables the use of seawater, as the vapor generated is free from salt contaminants.

Another alternative system proposes using a PEM electrolyzer supplied with a biomass aqueous solution on the anodic compartment and phosphoric acid on the cathodic compartment [76]. This innovative system has only been studied on a small scale but offers a critical advantage. Replacing the OER with a biomass oxidation anodic reaction leads to fewer thermodynamic constraints, thus enabling H_2 generation at lower cell voltages than conventional systems.

6. Conclusions

This work aimed to thoroughly analyze the fundamental concepts behind water electrolysis in acidic media, with particular emphasis on mechanisms and characterization parameters. It also analyzed PEM electrolyzer technology at both the cell and stack levels while providing insights into current cost breakdowns, identifying key manufacturers, and projecting future KPIs. Moreover, the emphasis on reducing the content of PGM materials as electrocatalysts for H_2 technologies has increased, driven primarily by the need to reduce overall system costs. The environmental impact and performance of this technology are also critical components in this context.

PEMEL, due to its ability to operate at high current density and achieve higher efficiencies, is seen as a fierce competitor to traditional alkaline water electrolysis. Currently, the electrolysis stack represents the second largest cost component in green H_2 production, accounting for approximately 45% of the total cost. This is primarily due to the manufacturing expenses associated with the components of the electrolyzers. Efforts to reduce

PGM content are not only economically important but also environmentally necessary. By reducing reliance on these materials, electrolyzer technologies have the potential to reduce their environmental impact while increasing their cost-effectiveness. Reducing the amount of PGM can be achieved through the implementation of strategies like forming alloys with abundant metals like Ni, Cu, Co, and Fe; downsizing Pt particles to increase the proportion of active surface sites, thus improving electrocatalytic efficiency and optimizing the use of PGM resources; homogeneously dispersing Pt on a support with high surface area and porous structure to take advantage of synergistic effects originating from the tunable Pt-support interaction; and modifying electronic structures through the regulation of compositions and material structure of Pt-based alloys or composites. These advancements underscore the importance of continuous research and development in optimizing PGM utilization, ultimately contributing to sustainable and efficient technological solutions for different applications.

In conclusion, the need to lower the price of PEM electrolyzers to produce green H_2 while focusing on reducing the dependency on critical raw materials like PGM materials highlights an essential turning point in the search for more sustainable alternatives. The growing demand for green H_2 presents a unique chance to accelerate the decarbonization agenda across multiple industries and sectors. By addressing the cost barriers associated with PEM electrolyzers, particularly by reducing the use of critical raw materials, the full potential of green H_2 for the energy transition can be realized.

Author Contributions: Conceptualization, J.A.G. and D.M.F.S.; methodology, J.A.G.; investigation, J.A.G.; writing—original draft preparation, J.A.G. and H.F.A.; writing—review and editing, H.F.A. and D.M.F.S.; supervision, D.M.F.S. All authors have read and agreed to the published version of the manuscript.

Funding: Fundação para a Ciência e a Tecnologia (FCT, Portugal) is acknowledged for funding a research grant in the scope of programmatic funding UIDP/04540/2020 (H.F.A.). FCT is also acknowledged for funding a Principal Researcher contract (2023.09426.CEECIND) in the scope of the Individual Call to Scientific Employment Stimulus—6th Edition (D.M.F.S).

Data Availability Statement: No new data were created or analyzed in this study.

Conflicts of Interest: The authors declare no conflicts of interest.

References

1. Ritchie, H.; Rosado, P.; Roser, M. Energy Production and Consumption. 2020. Available online: https://ourworldindata.org/energy-production-consumption (accessed on 29 June 2024).
2. United Nations: Climate Action Office. Renewable Energy: Powering a Safe Future. Available online: https://www.un.org/en/climatechange/raising-ambition/renewable-energy (accessed on 17 January 2024).
3. IRENA. Hydrogen: A Renewable Energy Perspective. 2022. Available online: https://www.irena.org/-/media/Files/IRENA/Agency/Publication/2019/Sep/IRENA_Hydrogen_2019.pdf (accessed on 17 January 2024).
4. Gómez, J.; Castro, R. Green Hydrogen Energy Systems: A Review on their Contribution to a Renewable Energy System. *Energies* **2024**, *17*, 3110. [CrossRef]
5. IRENA. Hydrogen: Overview. 2022. Available online: https://www.irena.org/Energy%20Transition/Technology/Hydrogen (accessed on 17 January 2024).
6. IRENA. Renewable Power Generation Costs in 2023. 2024. Available online: https://ourworldindata.org/grapher/levelized-cost-of-energy?facet=none (accessed on 17 January 2024).
7. IRENA. Green Hydrogen Cost Reduction: Scaling up Electrolyzers to Meet the 1.5 °C Climate Goal. Available online: https://www.irena.org/-/media/Files/IRENA/Agency/Publication/2020/Dec/IRENA_Green_hydrogen_cost_2020.pdf?rev=4ce868aa69b54674a789f990e85a3f00 (accessed on 17 January 2024).
8. IRENA. Green Hydrogen: A Guide to Policy Making. 2020. Available online: https://www.irena.org/-/media/Files/IRENA/Agency/Publication/2020/Nov/IRENA_Green_hydrogen_policy_2020.pdf (accessed on 17 January 2024).
9. Hydrogen Council. Hydrogen Insights 2023: An Update on the State of the Global Hydrogen Economy with a Deep Dive into North America. 2023. Available online: https://hydrogencouncil.com/wp-content/uploads/2023/05/Hydrogen-Insights-2023.pdf (accessed on 17 January 2024).
10. Salonen, L.M.; Petrovykh, D.Y.; Kolen'ko, Y.V. Sustainable Catalysts for Water Electrolysis: Selected Strategies for Reduction and Replacement of Platinum-Group Metals. *Mater. Today Sustain.* **2021**, *11–12*, 100060. [CrossRef]

11. Raveendran, A.; Chandran, M.; Dhanusuram, R. A Comprehensive Review on the Electrochemical Parameters and Recent Material Development of Electrochemical Water Splitting Electrocatalysts. *RSC Adv.* **2023**, *13*, 3843–3876. [CrossRef]
12. Wang, S.; Lu, A.; Zhong, C.-J. Hydrogen Production from Water Electrolysis: Role of Catalysts. *Nano Converg.* **2021**, *8*, 4. [CrossRef]
13. Li, W.; Tian, H.; Ma, L.; Wang, Y.; Liu, X.; Gao, X. Low-Temperature Water Electrolysis: Fundamentals, Progress, and New Strategies. *Mater. Adv.* **2022**, *3*, 5598–5644. [CrossRef]
14. Chatenet, M.; Pollet, B.G.; Dekel, D.R.; Dionigi, F.; Deseure, J.; Millet, P.; Braatz, R.D.; Bazant, M.Z.; Eikerling, M.; Staffell, I.; et al. Water electrolysis: From Textbook Knowledge to the Latest Scientific Strategies and Industrial Developments. *Chem. Soc. Rev.* **2022**, *51*, 4583–4762.
15. LibreText Chemistry. Redox Stability and Redox Reactions: 4.3 Electrochemical Potentials. Available online: https://chem.libretexts.org/Bookshelves/Inorganic_Chemistry/Book:_Introduction_to_Inorganic_Chemistry_(Wikibook)/04:_Redox_Stability_and_Redox_Reactions/4.03:_Electrochemical_Potentials (accessed on 29 June 2024).
16. Beswick, R.R.; Oliveira, A.M.; Yan, Y. Does the Green Hydrogen Economy Have a Water Problem? *ACS Energy Lett.* **2021**, *6*, 3167–3169. [CrossRef]
17. Morales-Guio, C.G.; Stern, L.-A.; Hu, X. Nanostructured hydrotreating catalysts for electrochemical hydrogen evolution. *Chem. Soc. Rev.* **2014**, *43*, 6555–6569. [CrossRef]
18. Shinagawa, T.; Garcia-Esparza, A.T.; Takanabe, K. Insight on Tafel Slopes from a Microkinetic Analysis of Aqueous Electrocatalysis for Energy Conversion. *Sci. Rep.* **2015**, *5*, 13801. [CrossRef]
19. Ma, Q.; Mu, S. Acidic Oxygen Evolution Reaction: Mechanism, Catalyst Classification, and Enhancement Strategies. *Interdiscip. Mater.* **2023**, *2*, 53–90. [CrossRef]
20. Zhang, Y.; Zhu, X.; Zhang, G.; Shi, P.; Wand, A.-L. Rational Catalyst Design for Oxygen Evolution Under Acidic Conditions: Strategies Toward Enhanced Electrocatalytic Performance. *J. Mater. Chem. A* **2021**, *9*, 5890–5914. [CrossRef]
21. Ossila. Linear Sweep Voltammetry: Introduction and Application. Available online: https://www.ossila.com/pages/linear-sweep-voltammetry (accessed on 29 June 2024).
22. Bockris, J.O.M.; Reddy, A.K.N.; Gamboa-Aldeco, M. *Modern Electrochemistry*, 2nd ed.; Kluwer Academic Publishers: Amsterdam, The Netherlands, 2000; p. 1107.
23. Anantharaj, S.; Karthik, P.E.; Noda, S. The Significance of Properly Reporting Turnover Frequency in Electrocatalysis Research. *Angew. Chem. Int. Ed.* **2021**, *60*, 23051–23067. [CrossRef] [PubMed]
24. Kempler, P.A.; Nielander, A.C. Reliable Reporting of Faradaic Efficiencies for Electrocatalysts Research. *Nat. Commun.* **2023**, *14*, 1158. [CrossRef] [PubMed]
25. IEA. Global Hydrogen Review. 2021. Available online: https://iea.blob.core.windows.net/assets/5bd46d7b-906a-4429-abda-e9c507a62341/GlobalHydrogenReview2021.pdf (accessed on 29 June 2024).
26. IEA. Electrolyzers. 2022. Available online: https://www.iea.org/energy-system/low-emission-fuels/electrolysers (accessed on 29 June 2024).
27. CATF. Solid Oxide Electrolysis: A Technology Status Assessment. 2023. Available online: https://www.catf.us/resource/solid-oxide-electrolysis-technology-status-assessment/ (accessed on 18 November 2024).
28. Shiva Kumar, S.; Himabindu, V. Hydrogen Production by PEM water electrolysis—A review. *Mater. Sci. Energy Technol.* **2019**, *2*, 442–454. [CrossRef]
29. Dincer, I.; Ishaq, H. Chapter 2—Hydrogen Production Methods. In *Renewable Hydrogen Production*; Dincer, I., Ishaq, H., Eds.; Elsevier: Amsterdam, The Netherlands, 2022; Volume 27, pp. 35–90.
30. Vidas, L.; Castro, R. Recent Developments on Hydrogen Production Technologies: State-Of-The-Art Review with a Focus on Green-Electrolysis. *Appl. Sci.* **2021**, *11*, 11363. [CrossRef]
31. Yuan, X.-Z.; Shaigan, N.; Song, C.; Aujla, M.; Neburchilov, V.; Kwan, J.T.H.; Wilkinson, D.P.; Bazylak, A.; Faith, K. The Porous Transport Layer in Proton Exchange Membrane Water Electrolysis: Perspectives on a Complex Component. *Sustain. Energy Fuels* **2022**, *6*, 1824–1853. [CrossRef]
32. Gómez, J.A.; Santos, D.M.F. The Status of On-Board Hydrogen Storage in Fuel Cell Electric Vehicles. *Designs* **2023**, *7*, 97. [CrossRef]
33. Yuan, X.-Z.; Shi, Z.; Song, C.; Xie, Z.; Zhang, L.; Zhao, N.; Girard, F. MEA-Membrane Electrode Assembly. In *Encyclopedia of Energy Storage*; Cabeza, L.F., Ed.; Elsevier: Oxford, UK, 2022; pp. 276–289.
34. Zhao, B.; Lee, C.; Lee, J.K.; Fah, K.F.; Lamanna, J.M.; Baltic, E.; Jacobson, D.L.; Husseym, D.S.; Bazylak, A. Superhydrophilic Porous Transport Layer Enhances Efficiency of Polymer Electrolyte Membrane Electrolyzers. *Cell Rep. Phys. Sci.* **2021**, *2*, 100580. [CrossRef]
35. Luo, X.; Ren, C.; Song, J.; Luo, H.; Xiao, K.; Zhang, D.; Hao, J.; Deng, Z.; Dong, C.; Li, X. Design and Fabrication of Bipolar Plates for PEM Water Electrolyzer. *J. Mater. Sci. Technol.* **2023**, *146*, 19–41. [CrossRef]
36. Grigoriev, S.; Millet, P.; Volobuev, S.; Fateev, V. Optimization of Porous Current Collectors for PEM Water Electrolysis. *Int. J. Hydrogen Energy* **2009**, *34*, 4968–4973. [CrossRef]
37. Laedre, S.; Kongstein, O.E.; Oedegaard, A.; Karoliussen, H.; Seland, F. Materials for Proton Exchange Membrane Water Electrolyzer Bipolar Plates. *Int. J. Hydrogen Energy* **2017**, *42*, 2713–2723. [CrossRef]
38. Rojas, N.; Sánchez-Molina, M.; Sevilla, G.; Amores, E.; Almandoz, E.; Esparza, J.; Cruz Vivas, M.R.; Colominas, C. Coated Stainless Steels Evaluation for Bipolar Plates in PEM Water Electrolysis Conditions. *Int. J. Hydrogen Energy* **2021**, *46*, 15929–25943. [CrossRef]

39. Lettenmeier, P.; Wang, R.; Abouatallah, R.; Saruhan, B.; Freitag, O.; Gazdzicki, P.; Morawietz, T.; Hiesgen, R.; Gago, A.S.; Friedrich, K.A. Low-cost and Durable Bipolar Plates for Proton Exchange Membrane Electrolyzers. *Sci. Rep.* **2017**, *7*, 44035. [CrossRef] [PubMed]
40. Bareiβ, K.; de la Rua, C.; Möckl, M.; Hamacher, T. Life Cycle Assessment of Hydrogen from Proton Exchange Membrane Water Electrolysis in Future Energy Systems. *Appl. Energy* **2019**, *237*, 862–872.
41. Patonia, A.; Poudineh, R. Cost Competitive Green Hydrogen: How to Lower the Cost of Electrolyzers. 2022. Available online: https://www.oxfordenergy.org/wpcms/wp-content/uploads/2022/01/Cost-competitive-green-hydrogen-how-to-lower-the-cost-of-electrolysers-EL47.pdf (accessed on 29 June 2024).
42. Global Market Insights: Insights to Innovation. PEM Electrolyzer Market—By Capacity (<500 kW, > 500 kW–2 MW, above 2 MW), by Application (Power Generation, Transportation, Industry Energy Industry Feedstock, Building, Heating Power) 2023–2032. Available online: https://www.gminsights.com/industry-analysis/pem-electrolyzer-market#:~:text=PEM%20Electrolyzer%20Market%20Size%20was,24.1%25%20btween%202023%20and%202032 (accessed on 29 June 2024).
43. Precedence Research. PEM Water Electrolyzer Market Size to Hit USD 13.12 bn by 2032. Available online: https://www.precedenceresearch.com/pem-water-electrolyzer-market (accessed on 29 June 2024).
44. Nel ASA. PEM Electrolyzer: PSM Series Specifications. Available online: https://nelhydrogen.com/wp-content/uploads/2024/03/PSM-Series_PD-0600-0141-Rev-C_Web.pdf (accessed on 13 September 2024).
45. H-TEC SYSTEMS. PEM Electrolysis Products: H-TEC PEM Electrolyzer Modular Hydrogen Platform. Available online: https://www.h-tec.com/en/products/detail/mhp-series/mhp-electrolyser/ (accessed on 29 June 2024).
46. Siemens Energy. PEM Electrolyzer: Electrolyzer Portfolio: The Optimum Solution for Large-Scale Sustainable Hydrogen Production. Available online: https://www.siemens-energy.com/global/en/home/products-services/product-offerings/hydrogen-solutions.html (accessed on 29 June 2024).
47. Cummins Inc. Hydrogen: The Next Generation Discover Cummins Electrolyzer Technologies. Available online: https://www.cummins.com/sites/default/files/2021-08/cummins-hydrogen-generation-brochure-20210603.pdf (accessed on 13 September 2024).
48. SinoHy Energy Co. Product: PEM Electrolysis. Available online: https://www.sinohyenergy.com/pem-electrolysis/ (accessed on 29 June 2024).
49. Plug Power Inc. The Plungex-4250d. Available online: https://resources.plugpower.com/electrolyzers/ex-4250d-f041122 (accessed on 29 June 2024).
50. Plug Power Inc. The Plugex-2125d. Available online: https://resources.plugpower.com/electrolyzers/ex-2125d-f041122 (accessed on 29 June 2024).
51. Elogen. Multi MW Electrolyzer. Available online: https://elogenh2.com/wp-content/uploads/2021/04/Elogen_Product_sheet-Multi-MW.pdf (accessed on 29 June 2024).
52. Keen Compressed Gas Cp. Hydrogen Conversion Data. Available online: https://keengas.com/gases/hydrogen/ (accessed on 29 June 2024).
53. Komanicky, V.; Latyshev, V. *Role of Electrocatalysts in Water Electrolysis*, 1st ed.; Springer Nature: Singapore, 2022; pp. 1–32.
54. Office of Energy Efficiency & Renewable Energy. Technical Targets for Proton Exchange Membrane Electrolysis: Hydrogen Fuel Cell and Technology. Available online: https://www.energy.gov/eere/fuelcells/technical-targets-proton-exchange-membrane-electrolysis (accessed on 29 June 2024).
55. Zhai, W.; Ma, Y.; Chen, D.; Ho, J.C.; Dai, Z.; Qu, Y. Recent Progress on the Long Term Stability of Hydrogen Evolution Reaction Electrocatalysts. *InfoMat* **2022**, *4*, e12357. [CrossRef]
56. Niu, H.; Wang, Q.; Huang, C.; Zhang, M.; Yan, Y.; Liu, T.; Zhou, W. Noble Metal Based Heterogeneous Catalysts for Electrochemical Hydrogen Evolution. *Appl. Sci.* **2023**, *13*, 2177. [CrossRef]
57. Li, Z.; Qi, Z.; Wang, S.; Ma, T.; Zhou, L.; Wu, Z.; Luan, X.; Lin, F.-Y.; Chen, M.; Millet, J.T.; et al. In Situ Formed Pt_3Ti Nanoparticles on a Two-Dimensional Transition Metal Carbide (MXene) Used as Efficient Catalysts for Hydrogen Evolution Reactions. *Nano Lett.* **2019**, *19*, 5102–5108. [CrossRef]
58. Bhuvanendran, N.; Park, C.W.; Su, H.; Lee, S.Y. Multifunctional Pt_3Rh-Co_3O_4 alloy nanoparticles with Pt-enriched surface and induced synergistic effect for improved performance in ORR, OER and HER. *Environ. Res.* **2023**, *229*, 115950. [CrossRef]
59. Zhang, Y.; Lan, J.; Xu, Y.; Yan, Y.; Liu, W.; Liu, X.; Gu, S.; Zhou, J.; Wang, M. Ultrafine PtCo alloy by pyrolysis etching-confined pyrolysis for enhanced hydrogen evolution. *J. Colloid Interface Sci.* **2024**, *660*, 997–1009. [CrossRef]
60. Bao, M.; Amiinu, I.B.; Peng, T.; Li, W.; Liu, S.; Wang, Z.; Pu, Z.; He, D.; Xiong, Y.; Mu, S. Surface Evolution of PtCu Alloy Shell over Pd Nanocrystals Leads to Superior Hydrogen Evolution and Oxygen Evolution Reactions. *ACS Energy Lett.* **2018**, *3*, 940–945. [CrossRef]
61. Domínguez-Crespo, M.A.; Ramírez-Meneses, E.; Torres-Huerta, A.M.; Garibay-Febles, V.; Philippot, K. Kinetics of hydrogen evolution reaction on stabilized Ni, Pt, and Ni-Pt nanoparticles obtained by an organometallic approach. *Int. J. Hydrogen Energy* **2012**, *37*, 4798–4811. [CrossRef]
62. Guo, K.; Zheng, J.; Bao, J.; Li, Y.; Xu, D. Combining Highly Dispersed Amorphous MoS_3 with Pt Nanodendrites as Robust Electrocatalysts for Hydrogen Evolution Reaction. *Small* **2023**, *19*, 2208077. [CrossRef]
63. Li, C.; Baek, J.-B. Recent Advances in Noble Metal (Pt, Ru, and Ir)-Based Electrocatalysts for Efficient Hydrogen Evolution. *ACS Omega* **2020**, *5*, 31–40. [CrossRef]

64. Cui, C.; Cheng, R.; Zhang, H.; Zhang, C.; Ma, Y.; Shi, C.; Fan, B.; Wang, H.; Wang, X. Ultrastable MXene@Pt/SWCNTs' Nanocatalysts for Hydrogen Evolution Reaction. *Adv. Funct. Mater.* **2020**, *30*, 2000693. [CrossRef]
65. Chen, Z.; Duan, X.; Wei, W.; Wang, S.; Ni, B.-J. Recent advances in transition Metal-Based Electrocatalysts for Alkaline Hydrogen Evolution. *J. Mater. Chem. A* **2019**, *7*, 14971–15005. [CrossRef]
66. Zeng, J.; Liu, Y.; Huang, Z.; Qiao, H.; Qi, X. Transition Metal Dichalcogenides in electrocatalytic water splitting. *Catalysts* **2024**, *14*, 689. [CrossRef]
67. Yu, J.; Li, Z.; Liu, T.; Zhao, S.; Guan, D.; Chen, D.; Shao, Z.; Ni, M. Morphology control and electronic tailoring of Co_xA_y (A = P, S, Se) electrocatalysts for water splitting. *Chem. Eng. J.* **2023**, *460*, 141674. [CrossRef]
68. Zhang, T.; Ren, X.; Cao, W.; Zou, H.; Jiang, X.; Ma, F.; Chen, R.; Qiao, H.; Zhang, Y.; Liu, H.; et al. Exploring 1T/2H MoS_2 quantum dots modified 2D CoP_x nanosheets for efficient electrocatalytic hydrogen evolution reaction. *J. Colloid Interface Sci.* **2025**, *679*, 569–577. [CrossRef] [PubMed]
69. Hu, C.; Xiao, Y.; Zou, Y.; Dai, L. Carbon-Based Metal-Free Electrocatalysis for Energy Conversion, Energy Storage, and Environmental Protection. *Electrochem. Energy Rev.* **2018**, *1*, 84–112. [CrossRef]
70. Wang, J.; Kong, H.; Zhang, J.; Hao, Y.; Shao, Z.; Ciucci, F. Carbon-based Electrocatalysts for Sustainable Energy Applications. *Prog. Mater. Sci.* **2021**, *116*, 100717. [CrossRef]
71. Zhou, F.; Zhou, Y.; Liu, G.-G.; Wang, C.-T.; Wang, J. Recent advances in nanostructured electrocatalysts for hydrogen evolution reaction. *Rare Met.* **2021**, *40*, 3375–3405. [CrossRef]
72. Guo, F.; Macdonald, T.J.; Sobrido, A.J.; Liu, L.; Feng, J.; He, G. Recent advances in ultralow-Pt-Loading Electrocatalysts for the efficient hydrogen evolution. *Adv. Sci.* **2023**, *10*, 2301098. [CrossRef] [PubMed]
73. Ge, J.; Zhang, D.; Qin, Y.; Dou, T.; Jiang, M.; Zhang, F.; Lei, X. Dual-metallic single Ru and Ni atoms decoration of MoS_2 for high-efficiency hydrogen production. *Appl. Catal. B Environ.* **2021**, *298*, 120557. [CrossRef]
74. Chi, J.-Q.; Xie, J.-Y.; Zhang, W.-W.; Dong, B.; Qin, J.-F.; Zhang, X.-Y.; Lin, J.-H.; Chai, Y.-M.; Liu, C.-G. N-Doped Sandwich Structured Mo_2C@C@Pt Interface with Ultralow Pt Loading for pH-Universal Hydrogen Evolution Reaction. *ACS Appl. Mater. Interfaces* **2019**, *11*, 4047–4056. [CrossRef] [PubMed]
75. Tang, J.; Guo, K.; Guan, D.; Hao, Y.; Shao, Z. A semi-vapor electrolysis technology for hydrogen generation from wide water resources. *Energy Environ. Sci.* **2024**, *17*, 7394–7402. [CrossRef]
76. Umer, M.; Brandoni, C.; Tretsiakova, S.; Hewitt, N.; Dunlop, P.; Mokim, M.D.; Zhang, K.; Huang, Y. Hydrogen production through polyoxometalate catalyzed electrolysis from biomass components and food waste. *Results Eng.* **2024**, *23*, 102803. [CrossRef]